WAAM processing of AISI 410 stainless steel for part building

João Miguel Araújo Bruno

Thesis to obtain the Master of Science Degree in

Mechanical Engineering

Supervisors: Prof. Inês da Fonseca Pestana Ascenso Pires

Prof. Carlos Manuel Alves da Silva

Examination Committee

Chairperson: Prof. Rui Manuel dos Santos Oliveira Baptista

Supervisor: Prof. Inês da Fonseca Pestana Ascenso Pires

Member of the Committee: Prof. Eurico Gonçalves Assunção

November 2019

Abstract

Wire and Arc Additive Manufacturing (WAAM) is an additive manufacturing process that is receiving increased attention from researchers and manufacturers. Making use of standard welding equipment, studies have shown that there is possibility that this process reveals itself to be quite an attractive replacement or complement for certain traditional manufacturing processes and thus carving its place in the 4th industrial revolution.

In this work, the feasibility of using a low carbon martensitic stainless steel, AISI 410, for WAAM processing using a CMT power source was investigated. After an initial stage of parametrization work, material characterization tests, namely, metallographic analysis, hardness tests and tensile tests, were performed and compared to the expected values found in literature and manufacturer technical data sheets. Microstructure and hardness were found to be in line with what was found in specialized literature, with metallographic analysis not revealing any of the common defects associated with martensitic structure. Tensile testing revealed that tensile properties were anisotropic, with samples perpendicular to direction of deposition showing greater strength (1235,15 MPa vs 1122,42 MPa), and samples parallel to direction of deposition showing greater ductility (0,10 vs 0,.7). After parametrization and material characterization, two CAD software's, Autodesk's PowerMill Additive and Cranfield's University WAAM Software, WAAMPlanner, were used for part deposition and the subsequent results were analyzed. Finally, a final part was deposited based on the best parameters and deposition strategy.

It has been shown that, using WAAM processing, it is possible to use a CAD software to design and deposit a part with high hardness and tensile strength, especially attractive properties to parts requiring high resistance to wear while in use.

Keywords: Wire and Arc Additive Manufacturing, DED+Arc, WAAM, AISI 410, martensitic stainless steel, CMT, WAAM Software, deposition strategies

Resumo

Wire and Arc Additive Manufacturing (WAAM) é um processo de fabrico aditivo que se encontra a receber cada vez mais atenção de investigadores e fabricantes. Utilizando equipamento de soldadura convencional, estudos efectuados têm demonstrado que existe uma possibilidade que este processo possa vir a ser uma alternativa ou complemento bastante atractiva a processos de fabrico mais tradicionais, estando a encontrar o seu espaço na 4ª revolução industrial.

Neste trabalho, foi estudada a viabilidade de utilizar um aço inoxidável martensítico com baixo teor de carbono, AISI 410, para processamento por WAAM com uma fonte de calor do tipo CMT. Após um trabalho inicial de parametrização, foram realizados ensaios de caracterização do material, nomeadamente, análise metalográfica, ensaios de dureza e de tracção. Os resultados destes ensaios foram posteriormente comparados com os valores encontrados na literatura e nas fichas técnicas do material fornecidas pelo fornecedor. A microestrutura e a dureza obtidas revelaram-se semelhantes aos das estruturas apresentadas na literatura da especialidade, com a análise metalográfica a não revelar quaisquer dos defeitos típicos associados a estruturas martensíticas. Os ensaios de tracção revelaram a existência de anisotropia nas propriedades mecânicas, com as amostras perpendiculares à direcção de deposição a demonstrarem maior resistência mecânica (1235,15 MPa vs 1122,42 MPa), e as amostras paralelas à direcção de deposição a demonstrarem maior ductilidade (0,10 vs 0,07). Após parametrização e caracterização do material, dois *software's* de CAD, *PowerMill Additive* da *Autodesk* e um *software* para WAAM desenvolvido pela Universidade de *Cranfield*, WAAMPlanner, foram utilizados para deposição de peças, com os resultados provenientes dessas experiências a serem devidamente analisados. Por fim, procedeu-se à deposição de uma peça final, tendo por base os melhores parâmetros e estratégia de deposição.

Este trabalho mostrou que, utilizando processamento por WAAM, é possível utilizar um *software* de CAD para desenhar e depositar uma peça com elevada dureza e resistência mecânica, propriedades especialmente atractivas para peças utilizadas em condições de serviço de elevado desgaste.

Palavras-chave: *Wire and Arc Additive Manufacturing*, WAAM, AISI 410, aço inoxidável martensítico, CMT, *software* para WAAM, estratégias de deposição

Acknowledgements

I would like to thank first of all Prof.ª Inês Pires and Prof. Carlos Silva for the opportunity, guidance and support given throughout this project.

I would also like to express my gratitude to the members of the Manufacturing and Process Technology Laboratory in Instituto Superior Técnico, in particular Ricardo Batista and João Pragana for their advice, comments and technical assistance which proved invaluable for the completion of this work.

I would also like to thank the "ADMIRE"- 575938-EPP-1-2016-1-UK-EPPKA2-KA project for the support given.

A special thanks to all my friends for their support and friendship along this journey.

Last, but perhaps most importantly of all, I would like to thank my parents and my sister for their continued support through my life. Thank you for being there in the good and, especially, in the bad moments.

Content

List of Figures

List of Tables

Acronyms

AM	Additive Manufacturing
ASTM	American Society for Testing and Materials
BTF	Buy to Fly
CAD	Computer Aided Design
CMT	Cold Metal Transfer
CTWD	Contact Tip to Work Distance
DED	Directed Energy Deposition
GMAW	Gas Metal Arc Welding
GTAW	Tungsten Arc Welding
HAZ	Heat Affected Zone
HV	Vickers Hardness
ISO	International Organization for Standardization
PAW	Plasma Arc Welding
SGFR	Shielding Gas Flow Rate
TM	Traditional Manufacturing
TS	Travel Speed
UTS	Ultimate Tensile Strength
WAAM	Wire and Arc Additive Manufacturing
WFS	Wire Feed Speed
WLAM	Wire and Laser Additive Manufacturing
WT	Waiting Time
YS	Yield Strength

1. Introduction

1.1. Motivation

In today's world, where industrial competition, locked in an ever-growing state, is faced with an increasingly environmentally conscious society, an economic pressure that forces manufacturers to do "more with less" and consumers demand for customized items, the need to reduce both costs and material waste, while keeping a flexible manufacturing approach has reached an all-time high. As a response to this need, Additive Manufacturing (AM) processes have begun to arise. Considered little more than a novelty when it first emerged, AM processing of materials have begun to find their place in the industrial environment, promising personalized items at no increased cost, shortening the supply chains and reducing the waste of material [1], [2].

Being one of the cornerstones of engineering applications, AM techniques for metal processing are being the focus of research, seeking to take advantage of the benefits brought by this technology. Among these techniques, Directed Energy Deposition (DED), and, more specifically Wire and Arc Additive Manufacturing (WAAM), is one that shows promise in an industrial environment. Being an arc-based process and using metallic wire as feedstock, this process builds upon vastly researched welding processes in an attempt to build increasingly complex parts while enjoying high deposition rates, reduced material waste and ease of access to the process itself [3].

When all of these factors are considered, it comes as no surprise that research in WAAM and AM in general is being increasingly researched and, expanding the range of materials that can be used by this technology will only lead to a larger field of applications. This is why there is a drive in researching this subject and contribute to the advancement of the manufacturing industry.

1.2. Thesis Objective

The main objective of this work was to determine the feasibility of employing an AISI 410 martensitic stainless steel in WAAM applications using a Cold Metal Transfer (CMT) power source to create parts using AM CAD software. In order to achieve this goal this work was divided in three distinct stages:

1. A preliminary parameterization study was carried out by depositing short single pass walls of six layers and analyzing their characteristics. This allowed to determine a set of parameters that produced geometrically sound walls.
2. Material characterization tests were performed to determine how the process affects the mechanical properties of this steel. Metallographic analysis, hardness tests and tensile tests were performed.
3. Designing and depositing a part using two different AM CAD software's and comparing the achieved results. A commercially available software, Autodesk's PowerMill Additive, and a beta version of a WAAM software being developed at Cranfield's University were used.

After conclusion of these stages a final part was deposited.

1.3. Thesis Structure

This thesis is divided in five chapters, with the following structure:

1. Introduction - This chapter outlines the motivation, contextualizing the problem that required addressing by this work. The thesis main objectives are also enumerated.
2. State of the Art - On this chapter a literature review of AM is performed, with a brief history of its evolution, the advantages and disadvantages against TM, the range of materials used. An overview of metal AM technologies is also provided with a special focus on DED technologies, mainly WAAM. Finally, an overview of the required functionalities of an WAAM Software is given, as well as brief analysis of the software's used during this work.
3. Material and Methodology - The material used in this work is identified and classified. The experimental setup and methodology of the different tasks undertaken during this thesis is also presented.
4. Results and Analysis - Data extracted from the various tests is provided and analyzed.
5. Conclusions and Future Work - Conclusions pertaining the developed work are presented and future work is proposed.

2. State of the Art

2.1. Additive Manufacturing

The American Society for Testing and Materials (ASTM) and the International Organization for Standardization (ISO) both define Additive Manufacturing (AM) as “a process of joining materials to make objects from 3D model data, usually layer upon layer, as opposed to subtractive manufacturing methodologies” [4]. This process is also known as additive layer manufacturing, rapid prototyping, freeform fabrication or, as it is most commonly called, 3D printing.

This form of manufacturing was first introduced in 1987 by an American company, 3D-Systems, with a process that was named stereolithography. This process subjected a light sensitive liquid polymer to ultraviolet radiation, in laser form, that would solidify it, layer by layer, in a set pattern to form a part.

In the following three years other companies, such as Sony from Japan and Electro Optical Systems from Germany, developed and sold their versions of stereolithography systems [5].

During this period this technology was mainly used for the rapid creation of models and prototypes which, unsurprisingly, earned it the name of rapid prototyping. Professions from various different fields still use it, from engineers and architects, to medical doctors, scientists and artists [6].

Across the following decades new AM technologies were developed and the range of materials usable for it was expanded from simply polymers, to metals and ceramics [7] and even biomaterials [8].

Nowadays, with the expiration of several patents related to the key AM processes [9], companies and investigators are researching and developing new ways this technology can be further expanded and find its place in the manufacturing industry.

2.1.1. Advantages

Before discussing the advantages AM has over traditional manufacturing (TM) methods it should be noted that the purpose of AM is not to replace them entirely, but rather complement them and provide more options for the manufacturing of parts and components.

AM has five key benefits over TM (see Figure 2.1) [1]:

- Cost
- Speed
- Quality
- Innovation / Transformation
- Impact

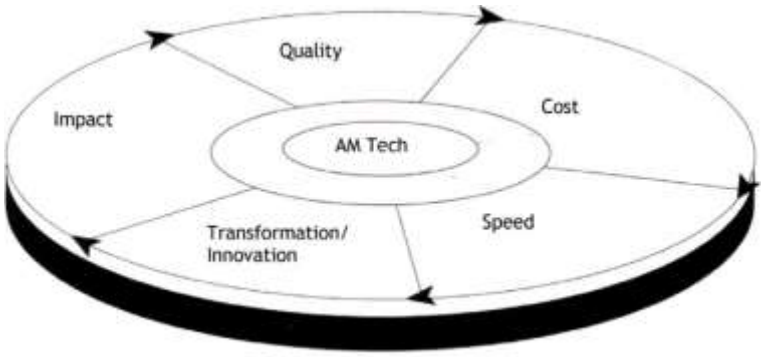

Figure 2.1 Five key benefits of AM over TM [1]

AM can allow consumers to produce replacement parts for their products locally, as long as a 3D printing file for the required part is available. This would be especially helpful when carrying out work in remote locations, not only increasing efficiency, since it would cut down shipping times (and costs), but also eliminate the need for large warehousing of components which is, in itself, quite costly as well.

Another advantage AM has over TM is the design flexibility it provides, since the fabrication of components layer by layer allows for a very wide range of geometric complexities. This flexibility comes from the lack of diverse tooling and collision awareness, both of them requirements for successful TM processing, as well as allowing easy access to interior features of the part being manufactured, which is not always the case in TM. This allows for modifications and redesigns of components without added penalties which, when considering that over 60% of designs submitted for tooling are modified while in production, is of extreme importance to reduce costs in both time and money [1].

The need for assemblage of components can also be eliminated in certain cases, since this technology is capable of producing complex complete systems that would otherwise require the assembly of several parts produced by TM [10].

Although it cannot be completely eliminated in some AM processes, the waste material associated with this technology can be severely reduced when compared to TM, resulting in very low buy-to-fly ratio, which is the weight of the raw material used to produce the component and the weight of the final component itself [2].

All of these factors combined contribute not only to reduce both monetary and time costs, but also to reduce the environmental impact of product manufacturing, which is an invaluable trait nowadays when industry as to be as environmental conscious as possible.

2.1.2. Disadvantages

Despite its advantages over TM, AM also has issues that prevent it from replacing TM completely.

Although very useful for producing custom parts or low volume series, AM is totally outclassed by other technologies when a high-volume series is required, mainly due to cycle time.

There is a relationship between the layer resolution and the scale of the parts being produced. When a higher layer resolution is used, which is equivalent to saying that a smaller layer thickness is used, the part ends up with a better surface finish, but, since more layers are required to build it, the total amount of time required to complete it also increases greatly. If the resolution is lowered enough to cut down on time costs an effect called the “stair-stepping” effect may become present, depending on the variant of AM used. Similar to an integral, this effect creates a poorly approximated curvature of the part, affecting surface finish [10].

Although post-processing can be used to smooth out the surface of the part, or to remove anchor or support material when the creation of overhang fixtures is required, this can be difficult to perform depending on the material and technology variant used, not to mention that it starts to increase time costs which is one of the advantages AM has over TM.

Another issue that affects AM is the limited selection of materials available. Even more limited is the capability of producing multi-material parts, although some studies have been performed on this area in polymer [11] and metal [12]. Despite these studies more research is still required in order to determine if multi-material parts can be achieved on all variants of AM.

The cost of the printing equipment and building material can also be quite high, although it is expected that with the increasing adoption of this technology by manufacturers, it will decrease in the future.

This decrease in costs creates another issue though. With increasing availability of this technology to the general public and with the existence of downloadable 3D project files, there is virtually no limit to what anyone can create in their own home. This will enforce a revolution on intellectual property protection or force companies to adapt in order to remain competitive and offer the best products. Some sort of regulation will also be needed to prevent weapons and other harmful products from being manufactured uncontrollably.

2.2. Materials

The materials for AM technologies have the same requirements as the ones used in TM: the feedstock must be formed into a state compatible with the process in question and its properties must be suited to the application where it’s going to be used [7].

Although still somewhat limited, the range of materials used in AM technologies is being expanded with the research and studies being carried out. In this section a summary of commonly used metals in AM processing is presented. Metals are mainly deposited by powder bed fusion and directed energy deposition techniques, although binder jetting is also used. At this time the following alloys are commercially available for use with AM processes:

- Ti6Al4V [13]–[16]
- 316L Stainless steel [17]–[19]
- 17-4PH Stainless steel [20]–[23]
- 18Ni300 Maraging steel [24], [25]

- AlSi10Mg [26]–[29]
- CoCrMo [30], [31]
- Inconel 718 and Inconel 625 [32]–[35]

Although this range is being continuously expanded it is still quite limited. This is due to the fact that if the metals are not weldable and castable they cannot be used in AM. Furthermore, the fusion of metals in contact with cold areas of the substrate introduce large thermal gradients that originate large residual stresses and undesirable microstructures. These issues may be too complicated to address in an efficient manner, which may invalidate the use of a metal in AM processes.

2.3. AM technologies

The ASTM and ISO both define seven AM categories [4], although only the metal processing by Directed Energy Deposition (DED) will be discussed. This section will be divided in two sub-sections. In the first a brief description of Directed Energy Deposition processes is provided and in the second a more detailed overview for the Wire and Arc Additive Manufacturing (WAAM) process will be provided, since it is the process that was used in this work.

Figure 2.2 provides an overview of the main metal AM processes [36]. These processes are divided first by their heat source, and second by the type of material feedstock employed.

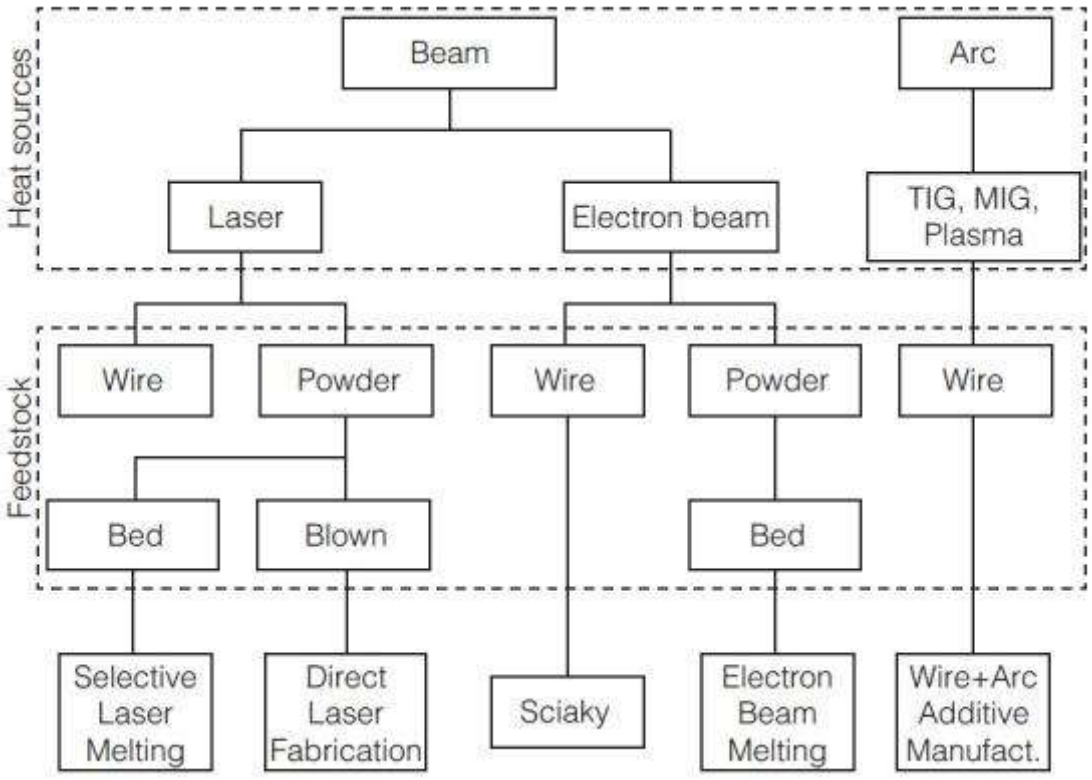

Figure 2.2 Main Metal AM Processes [36]

2.3.1. Directed Energy Deposition

DED is “An AM process in which focused thermal energy is used to fuse materials by melting as they are being deposited” [4]. This process makes use of an energy source, usually in the form of a laser beam, electron beam or electric arc, to melt and deposit metal, fed in wire or powder form, onto a substrate. The energy is focused at a narrow zone, which creates a melt pool in the substrate and melts the material, that, after cooling down, will create a layer of the part. Depending on the material, the rapid heating and cooling of the deposits can originate a build-up of residual stresses that can lead to defects in the finished part, which can be reduced by using heat or mechanical treatments [37].

This process can be divided into two categories depending on the feedstock. The first category uses powder as feedstock, and it’s called Direct Laser Fabrication. Passing through a system of lenses, a laser beam focuses a spot of the building platform while metal powder is injected at that spot. As the powder is fed into the melt pool, a layer is created through the movement of the building platform and the solidifying of the injected material. This process repeats until the part is finished [38].

The second category, which uses wire as feedstock, can be divided in three processes, depending on the heat source used (see Figure 2.2). Electron Beam Direct Melting is a process developed by NASA, similar to EBM. Requiring a vacuum environment to be properly applied, and using a wire as feedstock, makes this process ideal for use in space based applications, where the use of powder is complicated due to low gravity conditions [9]. Another process of wire fed DED technology is Wire and Laser Additive Manufacturing (WLAM). This process makes use of a wire feeder system, a laser and a robotic system or movable table to melt and deposit material in a controlled fashion to create parts [37]. Finally, there is the Wire and Arc Additive Manufacturing (WAAM) process. This process makes use of the same equipment as WLAM, substituting the laser for an arc welding system as heat source, this process can offer higher deposit rates while enjoying lower equipment costs [37]. The WAAM process was selected to be used in this work and it’s described in further detail in section 2.3.2

2.3.2. Wire and Arc Additive Manufacturing

As stated in the previous section, WAAM is a DED AM process that makes use of standard welding equipment, as a heat source, to melt and deposit metal, fed in wire form, to manufacture parts. Despite being patented in 1925 [39], WAAM process only started to be under investigation as an AM process since the early 1990’s [40].

2.3.2.1. Welding processes used in WAAM

Although the use of automatized welding processes like Gas Metal Arc Welding (GMAW), plasma arc welding (PAW) and tungsten arc welding (GTAW) are all available, GMAW is the preferred process whenever this DED category is employed. The popularity of GMAW in WAAM is related with the coaxiality of the wire, that acts as the consumable electrode, with the welding torch, providing an easier toolpath for the deposition [41], which increases the efficiency of the process. GMAW can employ inert

or active gases depending on the metal being used. With reactive alloys, such as aluminums, being deposited, inert gases should be used to take advantage of the inert atmosphere they provide through the use of Argon (Ar) or Helium (He) as the shielding gas. Active shielding gases, like Carbon Dioxide (CO_2) or Oxygen (O_2) are used to deposited mainly steels, providing the protective atmosphere for the weld pool. With a wide range of deposition rates, from 15 to 160 g/min [42], this welding process is very attractive for the creation of large parts in a reasonable amount of time. See Figure 2.3 - (a) for a schematic of the process [43].

A variant of GMAW developed by Fronius©, known as cold metal transfer (CMT), is also highly attractive for use in AM. With a controlled dip transfer mode mechanism, where the electrode wire tip retracts and advances, through the use of a servomotor, when it contacts the melt pool, Fronius claims that the deposited beads present higher quality, with less spatter and lower heat input [44]. While these claims hold true when depositing aluminum and steel [45], the process is affected by arc wandering when depositing titanium, which leads to high surface roughness [46], although it has been found that, when properly optimized, it can in fact be used for these titanium based alloys [41].

The other available processes, GTAW and PAW, share some similarities in their nature. Both using a non-consumable tungsten electrode to generate their electric arc, with an inert gas, usually Argon, protecting the weld pool. Both of these processes can be used without filler material, however, for WAAM, they obviously require it, but since they can't be fed through the torch like in GMAW, they have to be fed externally, which leads to increased difficulties in robot programming, since wire fed angle and positioning has to be kept according to certain parameters to ensure adequate deposition [47]. Figure 2.3 – (b) and Figure 2.3 – (c) shows a schematic of the processes.

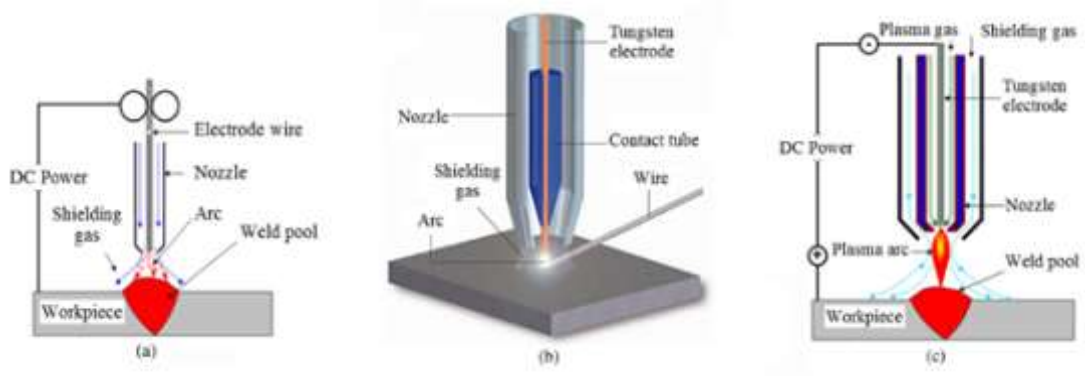

Figure 2.3 Schematic of the different WAAM welding processes: (a) GMAW, (b) GTAW, (c) PAW [50]

2.3.2.2. Materials used in WAAM

The feedstock used in WAAM is wire, which means that, theoretically, any material available in this form can be used for WAAM processing. However, in practice, the most used metals are steel, aluminum, titanium and nickel based alloys [42].

Being a staple in aeronautical industry, titanium and nickel-based alloys are garnering the interest of several researchers due to the possibility of lowering the high costs of processing these materials.

The processing of aluminum alloys by WAAM is challenging due to problems associated with the welding of this material. The formation of alumina during the building process and the introduction of porosity associated with the welding of aluminum require tight optimization of the process in order to produce suitable parts.

Enjoying a widespread use in various fields of industry, like automotive, nautical and construction to name a few, steels can be processed with WAAM to produce parts with low costs and reduced wastage of material. Stainless steels, have also been successfully employed in WAAM applications, with austenitic stainless steels enjoying particular attention [67–69]. However, due to the wear resistance of the martensitic grades, the interest of using this material as filler in WAAM is increasing, despite the difficulties needed to overcome when welding metal with such structure [51].

2.3.2.3. Wear resistant materials

Martensitic stainless steels present high wear resistance. Due to this nature, it is relevant to analyze the current studies on wear resistance of parts manufactured by WAAM.

Although no study on WAAM processed AISI 410 was found, Amrei *et al.* [52] carried out a study on multipass welding for this material. They observed a complex and heterogeneous microstructure, with several regions affected by adjacent weld beads, which also led to a variation of hardness values across the weld beads, with values ranging from 340 HV to 400 HV.

A number of researches on the wear properties of different materials processed WAAM has already been carried out. Wang *et al*. [53] studied the properties of AISI H13 steel and discovered that, for thin walled structures, Vickers hardness was kept uniform across the height of the samples, assuming values between 300 and 360 HV, high values that correlate to a high wear resistance for this material. Tensile testing performed in two different orientations also showed that mechanical properties were anisotropic, with a mean tensile strength and elongation of 1085 MPa and 10%, respectively for horizontal specimens and 871 MPa and 7,8% for vertical specimens.

Xu *et al.* [54] studied the deposition of a MARVAL 18S maraging steel by WAAM. They observed that a significant difference in hardness, from 330 HV at the bottom to 430 HV at the top, was present along the height of the part, due to the aging effect from each successive deposition. This difference was eliminated after aging the part and the hardness value increased, reaching 550 HV, suggesting that incorporating aging treatment could be very beneficial to the production of wear resistant steel parts. As for tensile properties, a UTS of 1165 MPa and an elongation of 13,7% were observed.

Besides steels, Yangfan *et al.* [55] researched the effect of WAAM deposition on Inconel 625 mechanical properties. Like the aforementioned studies, they concluded that Vickers hardness values are not uniform across height of the samples, although, unlike the previous studies, they observed that the values for hardness decreased along the samples, from 264 HV near the substrate to an average value

of 249 HV for the top region, and afterwards they increased again from this top region until the last layer where values of 260 HV were reached. Their explanation for this phenomenon is that the microstructure varies along the height of the sample, with a fine cellular structure near the bottom and coarser dendritic crystals at the top, consequence of heat accumulation along the successive depositions.

Attar *et al.* [56] studied the effect of three different AM processes for the deposition of titanium. Their study showed that all AM processing of the material led to an increase in hardness of the part when compared to parts produced by casting. However, from all the AM processes considered (SLM, LENS and WAAM), WAAM showed the lowest value for hardness, reaching 190 HV, while the largest, 229 HV, was achieved by SLM.

2.3.2.4. Advantages and Challenges in WAAM

One of the major advantages of WAAM is the fact of being able to achieve high deposition rates when compared to other metal AM technologies, with rates of 1 kg/h for aluminum and 4 kg/h for steel [3]. This characteristic allows to produce large parts in a reasonable amount of time, which is probably the most attractive feature of WAAM in the manufacturing industry. Even higher deposition rates can be achieved, up to 10 kg/h, but the quality of the part suffers degradation. The part size, for aluminum and steel, is only limited by the movement range of the motion system, while for titanium alloys the part size is limited by the extent of the chamber used to create the required inert atmosphere.

The costs of the basic WAAM equipment is also a point in its favor, with 100,000€ being enough to purchase a system capable of depositing both aluminum and steel, with titanium alloys requiring an extra purchase of a chamber to provide a suitable atmosphere for its deposition. These costs can be further reduced if manufacturers make use of already available equipment, since any brand of power source can be used with any brand of motion system.

Using wire as feedstock also has its advantages. It's a cheap form of feedstock, and, by using wire, many of the issues associated with the use of powders are avoided. The chance of contamination is also reduced since the wire is completely molten when deposited, becoming part of the final structure of the part.

Material waste is also low when compared with TM p, with most of the deposited raw material being present in the final product. As mentioned before, the BTF ratio of AM technologies can be significantly lower that of TM technologies, which is especially important when processing expensive materials such as titanium alloys. Considering that 15% of the total weight of the Boeing 787 is composed of such alloys, achieving these low BTF ratios is especially important in order to keep costs down [57].

Observing Figure 2.4, we can see that, compared with other AM technologies, DED processes, which WAAM is part of, present higher energy requirements than any other process, although it also offers the fastest deposition speed with average part resolution.

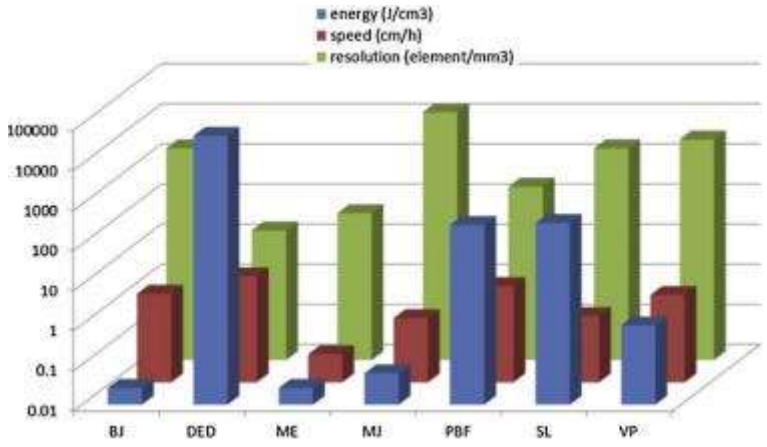

Figure 2.4 Comparison between AM technologies [73]

Going in further detail, Figure 2.5 shows us that WAAM holds the advantage in many key aspects of manufacturing, such as mechanical properties, cost savings and build rates, when compared to other metal AM processes, thus making it highly attractive for industrial applications [59].

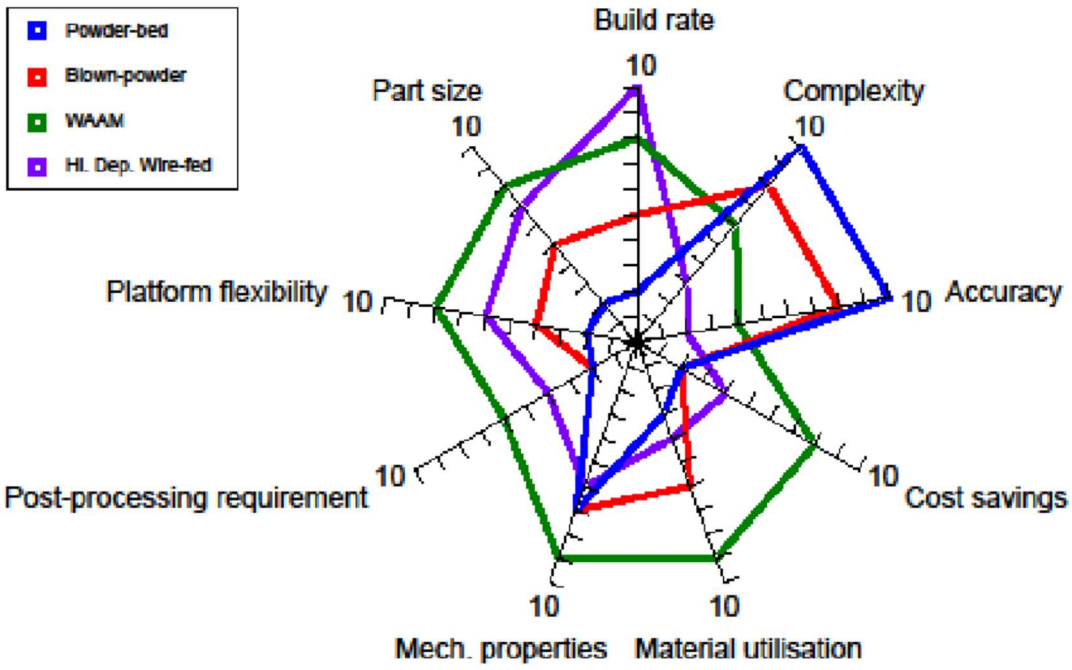

Figure 2.5 Comparison between different metal AM processes [59]

One of the major concerns of this technology is mainly related to the high level of residual stresses, associated with the high heat input characteristic of welding processes used in WAAM, which may create distortions, that will affect the accuracy of the part, when the clamping components are removed [60]. There are a few strategies to address to mitigate residual stresses, such as symmetrical building, back

to back building, part orientation and deposition strategy optimization and high pressure interpass rolling. [3].

Additionally, there are other two factors that affect part accuracy; one, that has been mentioned in section 2.1.2, is the stair stepping effect and the other one is the un-match effect. The un-match effect occurs when the sliced model with a constant layer thickness, which is how a solid is normally sliced, does not match the original model [2]. Adaptive slicing strategies have been developed to address this issue, where the layer thickness is adjusted automatically to ensure the shape of the model is as intended. Figure 2.6 shows an example of this effect and how adjusting the layer thickness solves the un-match effect.

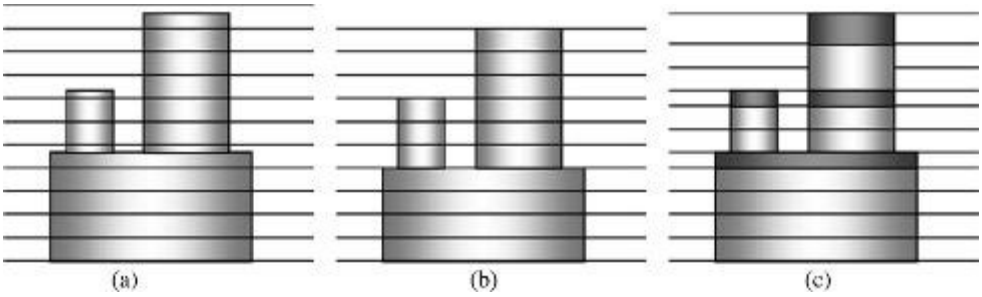

Figure 2.6 Layer thickness adjustment: (a) original model, (b) sliced model with constant layer thickness, (c) sliced model with adjusted layer thickness [50]

The stair stepping effect occurs when depositing layers with large thickness. This holds the advantage of speeding up the build process at the cost of dimensional accuracy. The higher the layer thickness the more this error adds up. So, when using WAAM with high deposition rates it's best to stick to simpler geometries or employ a milling process to improve the surface quality of the part [2]. Figure 2.7 shows an example of this effect.

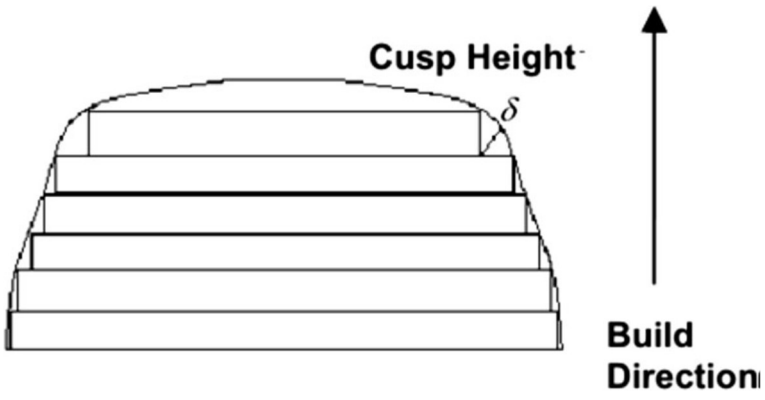

Figure 2.7 Stair stepping effect [50]

Surface finish of the part is also affected by the distance between two consecutive weld beads. Since weld beads have a curve similar to a parabola some overlap between them is required in order to produce a flat surface with multiple beads welded together. Several studies have been carried out in

order to determine the optimal relation between welding parameters and bead geometry. Figure 2.8 shows a sketch of how the overlap between beads affects the surface of the part. This topic is further analyzed in the deposition strategies sub-section 2.3.2.5.

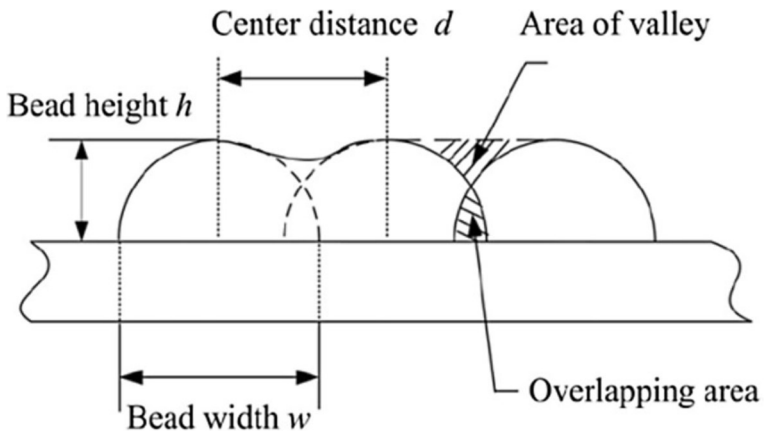

Figure 2.8 Sketch of traditional flat-top overlapping model [50]

2.3.2.5. Deposition strategies

Having in consideration that one of the main objectives of this work is the construction of a part by WAAM, deposition strategies are of paramount importance in order to produce defect free parts. In this sub-section a review of the current employed strategies in WAAM is carried out.

One of the most evident issues when depositing single walls is presented in Figure 2.9, where it can be seen that although the end result was supposed to be a flat top surface, the starting and ending height present a considerable difference between them. This happens when the start and end point are the same for every layer, where excessive heat sink at the initial deposition point causes lack of weld penetration, creating an increase in layer height. On the opposite side, at the final deposition point, low heat dissipation, due to the high temperatures associated with the welding process, cause a drop in layer height [42]. This error will be accumulating throughout the building process, creating a considerably large difference between extremities.

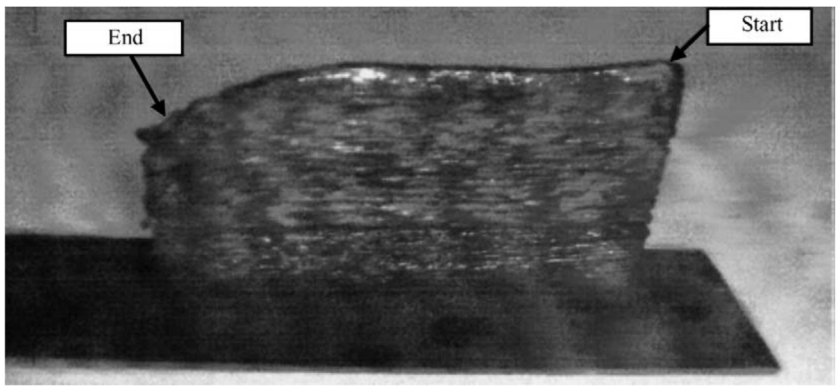

Figure 2.9 Example of single wall deposition [60]

Two methods are currently employed to overcome these differences. One of them is to control the current and travel speed of the torch, increasing them at the starting deposition point and reducing them at the end point [61]. It can be seen in Figure 2.10 that applying this procedure completely solved this geometrical problem.

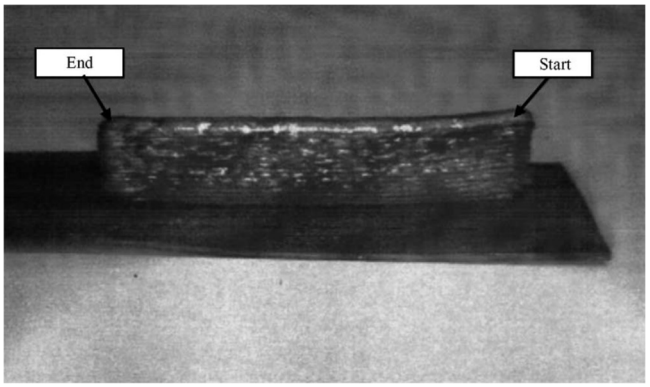

Figure 2.10 Example of single wall deposition with process parameter control at the start and end point [60]

The other method employs a “zig-zag” motion of the torch where the start and end point of deposition changes with every layer [62]. It can be seen in Figure 2.11 that this method also solves the problem in a satisfactory manner, but it can also result in high residual stresses at the wall boundaries, due to thermal accumulation in certain zones [42]. A workaround for this geometric inconsistency can be considering the starting and ending areas as sacrificial zones to be removed.

Figure 2.11 Deposition of single wall: (a) start and end point unchanged, (b) zig-zag motion [61]

As stated before, understanding weld bead geometry and its relation to the process parameters is also of extreme importance to obtain a defect free part. Researchers have tried to correlate welding parameters and bead geometry by regression analysis [63], artificial neural networks or combinations of these two techniques [64]. Researchers have determined that the optimal model of bead profile was dependent of the ratio between wire feed speed and travel speed of the torch, by comparing measured weld bead deposited with different welding parameters and three bead profile models [65]. Multi-bead

overlap models have been carried out. Figure 2.8 describes one of them, where the distance *d* between bead centers plays a pivotal role in obtaining a flat surface. If this distance is too large then there is no overlap between beads and, if it's too small there is an excessive overlap between beads, both situations are not ideal when depositing adjacent beads. The solution is to pick a value for *d* where the area of the valley and the area of the overlap is the same and a flat surface is achieved [65]. Although this should work theoretically, experimentation has shown that this does not work [63], due to undesired surface waviness that accumulates with successive layers. Recently a method has been proposed to obtain a more stable overlap when depositing steel, where it was shown that a distance *d* of 0.738 multiplied by the width of a bead produced a satisfactory flat surface [66].

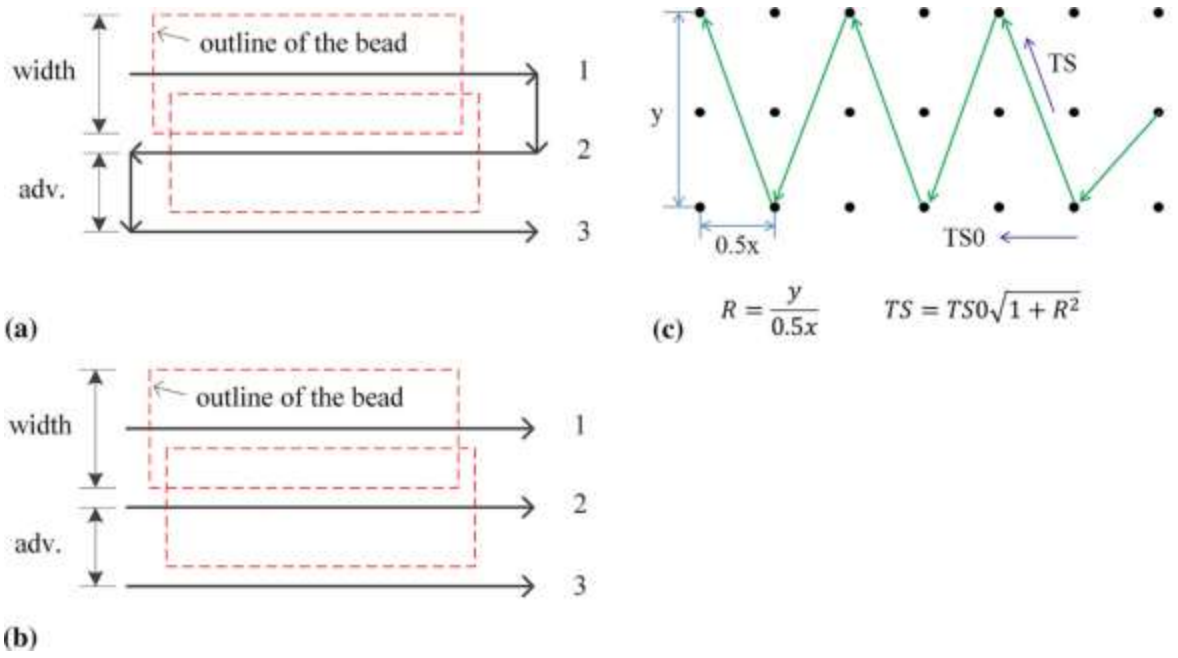

Figure 2.12 Deposition strategies carried out in [66], (a) Oscillation, (b) Parallel, (c) Weaving

Another study was carried out where the effect of three different deposition strategies on surface waviness and porosity in steel was carried out [67]. The three strategies were oscillation, parallel and weaving (see Figure 2.12). In this study it was determined that employing a weaving strategy not only resulted in a better surface finish, with a flatter top, which requires less machining after deposition, but also led to a decrease in porosity in the welds.

Regarding the decomposition of CAD models, studies seeking to minimize the number of start and stop of the torch and weld intersections have been carried out. One of them decomposed layers in polygons, filling each area and generating a closed loop toolpath [68]. Another method that has been developed, where the geometry of a slice plane is divided in a set of bisector segments. When these segments connect at more than two points they become branch points, with the depositions paths being generated around the segments connected by them [69].

The manufacturing of 90º walls has also been investigated. The developed strategy consisted in applying two complementary strategies, building four layers with the first one and using the second one to correct the geometry [70]. These strategies are presented in Figure 2.13.

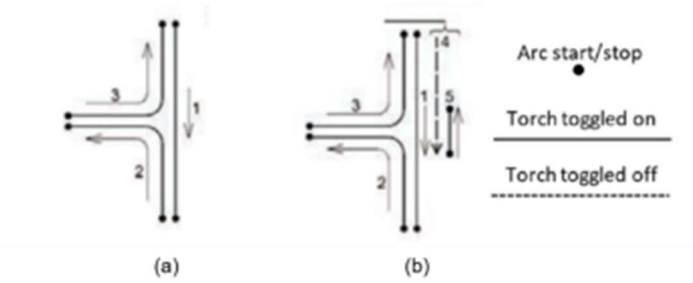

Figure 2.13 Strategy for T-type structures (a) – first strategy, (b) – second strategy [70]

2.4. WAAM Software's

Although the robotic systems used to produce large and complex parts by WAAM are available, the programming of such systems can be very time consuming, invalidating their use for industrial purposes. For this reason, software's that generate tool paths from a 3D CAD model for deposition are required. Actually, there is an effort to develop this kind of programs, either based on existing subtracting software or made from scratch, based on the knowledge acquired with the Metal AM technology.

Independently of the route taken on software development, in order to automize the tool path as much as possible, a WAAM software must be able to:

1. Select the most appropriate build strategy according to the geometry of the part;
2. Vary the process parameters during part deposition, based on the geometry and material. For that to happen a database of processes parameters for different materials would be required;
3. Partition the part in a way that minimizes the number of starts and stops of the system and the number of intersections in the deposition process;
4. Select the most appropriate building strategy for each individual partition in each layer
5. Check for collisions and error during the process
6. Automatically export a code that the robot system can read

Currently, Autodesk's PowerMill additive is a plugin of the commercially available PowerMill software that enables the creation of toolpaths for additive or hybrid manufacturing, that is driven by directed energy deposition. Although it is possible to build parts depositing material layer by layer, the process is not as streamlined as it could be, having limited building strategies available, no database of parameters and being difficult or outright impossible to customize the partition of the parts. At the moment, this software is best suited to produce simpler parts.

A WAAM Software is also being developed at Cranfield University and seeks to answer all of these issues. Despite already offering a larger degree of control over the process than PowerMill, this software is under a development stage, which means that some features are yet to be implemented. Current

limitations include manually partition of the part, limited to the oscillation strategies and the parameter database is still incomplete. This work will also be focused on the potential of PowerMill Additive and WAAM software to produce the martensitic stainless-steel part in study.

A description on how to operate each program is provided in section 3.7.

2.5. Summary

From the reviewed literature it can be stated that WAAM is a technology that provides many advantages over traditional manufacturing processes, mainly in a logistic and economic point of view, when taken into account the characteristics of this manufacturing process. However, some challenges, such as residual stresses, distortions and lack of standardization, still need to be tackled in order to be able to fully implement it into an industrial stage. In addition, lack of guidelines for part fabrication, fully fledged software focused on WAAM and availability of commercial systems, also needs to be addressed before AM can be used as complement or alternative for TM.

The present work aims to provide a contribution for the development of WAAM for part fabrication, making use of CAD software and AISI 410 steel, optimizing strategies of deposition and parameters to achieve a complete part.

3. Material and Methodology

In this chapter information related to the material and equipment used during this work is provided as well as an explanation of the different methodologies followed to build parts and carry out the different tests for material characterization.

3.1. Material

The material used for this work was a martensitic stainless steel, OK Autrod 410NiMo. It was supplied in wire form, by ESAB, with a diameter of 1.2 mm, in a 15 Kg spool. The data sheet of the material can be consulted in Appendix A.

The substrate material was low carbon steel, cut in a flat plate with dimensions: 250 x 200 x 15 mm. The substrate was grinded with an angle grinder to remove the oxide layer.

In Table 3.1 the chemical composition of the filler wire is provided.

Table 3.1 Chemical composition of OK Autrod 410NiMo steel

Material	Chemical composition %						
	C	Mn	Si	Ni	Cr	Mo	Cu
410NiMo	0.02	0.5	0.4	4.2	12.4	0.6	0.1

Like all martensitic steels, AISI 410 possesses high corrosion resistance, high strength and high toughness. Due to its low carbon content of 0.02% it is considered a supermartensitic stainless steel and it is used in various industries for the fabrication of essential parts, such as parts for computer hard drives, plastic moulds, screws, valves, shafts, bearings and pipelines as an alternative to austenitic and duplex stainless steels [71]. Table 3.2 shows the typical properties of this material in the “As welded” condition.

Table 3.2 Typical Properties of AISI 410NiMo steel in the “As welded” condition

Property	Value
Yield Strength	860 MPa
Ultimate Tensile Strength	1050 MPa
Elongation	13 %
Vickers Hardness	450 HV

3.2. Equipment Setup

The deposition work was performed at IST using a 6-axis KUKA robot coupled with a Fronius CMT welding power source. The shielding gas used for the deposition work was ARCAL Chrome with a mixture of Ar+2%CO_2 – ISO 14175-M12-ArC-2. The substrates were clamped to a steel table.

This setup is presented in Figure 3.1.

Figure 3.1 Deposition work setup

1. KUKA Robot
2. Torch
3. KUKA Robot Controller
4. CMT Power Source Controller
5. Wire Feeder
6. CMT Power Source
7. Shielding Gas Bottle
8. Exhaust Ventilation System
9. Substrate
10. Clamps

3.3. Deposition Parameters and procedure for linear walls

Two sets of depositions were carried out in order to determine the process parameters to be used to produce a more complex part.

The first set of experiments consisted in single bead walls with six layers each and 100 mm in length, created with a zig-zag motion of the torch, meaning that the start point changes with every consecutive layer (see Figure 2.11). The followed methodology for this deposition was to vary one parameter, while keeping all the others constant, in order to ascertain the effect that parameter has on the quality of the deposition.

The Shielding Gas Flow Rate (SGFR) and Contact Tip to Work Distance (CTWD) were kept constant throughout all depositions. The Wire Feed Speed (WFS) was varied in a range of values allowed by the welding machine controller. The other varied parameter was the Travel Speed (TS) of the torch, computed from a range of ratios WFS/TS. This ratio also provided an indication of the volume of deposited material, with higher ratios indicating higher volume of material. The current and voltage were set automatically by the welding machine, and its values were dependent on the selected material curve and WFS set on the controller.

A waiting time (WT) between layers was also employed, to allow for cooling, and it was set at 2 minutes between each layer. After each wall an evaluation based on visual inspection was carried out in order to divide the depositions into acceptable quality and not acceptable quality. The walls classified as acceptable were later used to prepare samples for metallographic analysis.

The second set consisted in walls created with an oscillation strategy (see Figure 2.12 – b), also with 6 layers and 50 mm in length. This second study was carried out after verifying the parameters defined previously for the single bead walls, are not suitable when producing walls with an oscillation strategy. Therefore, the same methodology was followed to determine a new set of parameters that could provide a solution to these problems.

These depositions were measured with a set of calipers. Three measurements were taken in order to calculate average width and thickness, two of them near the extremities and the other one in the center.

The results of these studies are presented in section 4.1.

3.4. Metallographic Analysis

The first step in sample preparation for metallographic analysis is to cut a small section of the deposited walls with about 20 mm in length, to mount them into the cylinder moulds. This work was carried out at IST using a mechanical saw.

The next steps were carried out at Instituto de Soldadura e Qualidade (ISQ).

The previously cut sections were hot mounted into cylinder moulds using a Struers LaboPress-3 machine.

The samples were grinded with various grit size sandpapers, ranging from 80 grit size to 1000 grit size, using a Struers Labopol. With the same equipment, the samples were polished with two different cloths and an abrasive agent. Finally, the samples were etched with Villela reagent by an ISQ member. The microstructure was then investigated under an optical microscope while a conventional scanner machine was used to obtain the macrostructure.

The data acquired from these tests is analyzed in section 4.2.1.

3.5. Hardness Tests

The specimens prepared for microscopic analysis were also used for hardness measurements allowing to analyze the evaluation of hardness along the direction of depositions due to the imposed thermal cycles and heat accumulation. The identification of distinct types of microstructure along the samples was also possible.

Hardness indentations were made with a Struers Duramin available at IST. The indentations were performed under a load of 5 N for 10 s per point in different zones of the samples along the height of the sample, obtaining 10 points per sample, spaced 1 mm between them, while also taking points from the Heat Affected Zone (HAZ).

With the hardness measurements it is also possible to estimate the Ultimate Tensile Strength (UTS) and Yield Strength (YS) of the deposited material. The values for UTS and YS can be estimated from the Vickers Hardness (HV) values through the correlation explained in [72]. This correlation was obtained through linear regression with a coefficient of determination R^2 of 0.9212 and a standard error of 102 MPa for YS and an R^2 value of 0.9347 and standard error of 112 MPa for UTS and states that:

$$YS = -90.7 + 2.876HV \tag{3.1}$$

$$TS = -99.8 + 3.734HV \tag{3.2}$$

These estimations were then compared to values for UTS and YS obtained from the tensile tests performed.

3.6. Tensile Tests

Tensile tests were carried out accordingly to the ISO 6892-1:2016 [73] standard.

To produce the specimens according to the standard, walls have to be made with at least 100 mm in height and 12 mm wide. To accomplish this goal a weaving motion had to be employed in combination with the best set of parameters obtained in the first deposition study, using a linear motion, that also produced the thickest walls. The weaving strategy consists of depositing according to a pattern set in

the program code instead of merely depositing linearly. The triangular weaving pattern with the following parameters was used to achieve walls with the required dimensions:

- Weaving amplitude: 6 mm
- Weave length: 4 mm
- TS: 0.256 m/min
- WFS: 6 m/min

Figure 3.2 shows a visual explanation of the different weaving pattern and respective parameters:

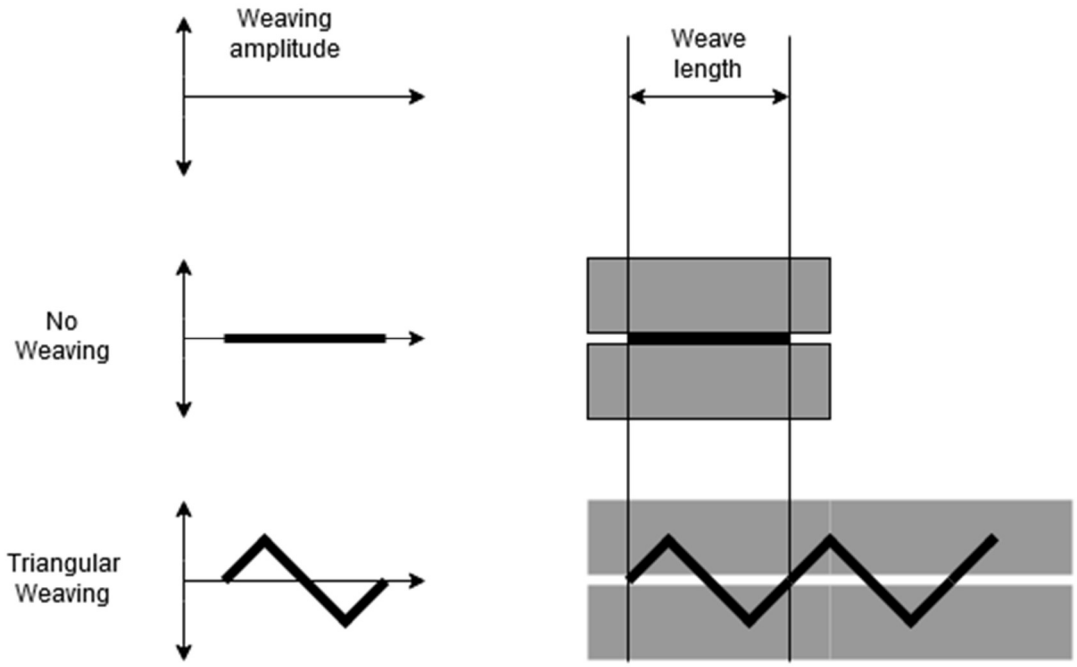

Figure 3.2 Weaving pattern and parameters

Tensile tests were made with an INSTRON Universal Testing Machine with a 200 kN cell available at the mechanical testing laboratory at IST. The elongation was measured by an extensometer placed on tensile specimens. Tests were performed with a load speed of 1 kN/min, following a ramp function, until reaching yield stress, and afterwards a constant speed of 5 mm/min until finishing the test.

Two sets of walls were deposited in order to extract samples in both orientations (see Figure 3.3). The samples were manufactured according to the ISO 6892-1:2016 standard. Two longitudinal (parallel to deposition direction) and four transversal samples (perpendicular to deposition direction) with dimensions given in Figure 3.4 were removed from each wall manufactured from the zones depicted in Figure 3.3.

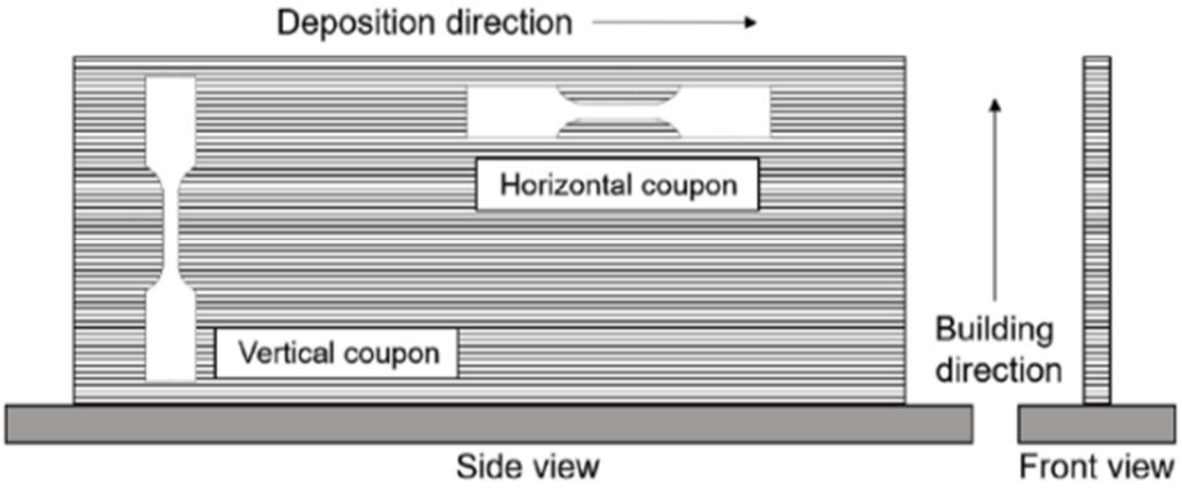

Figure 3.3 Orientation of tensile samples in relation to deposition direction [74]

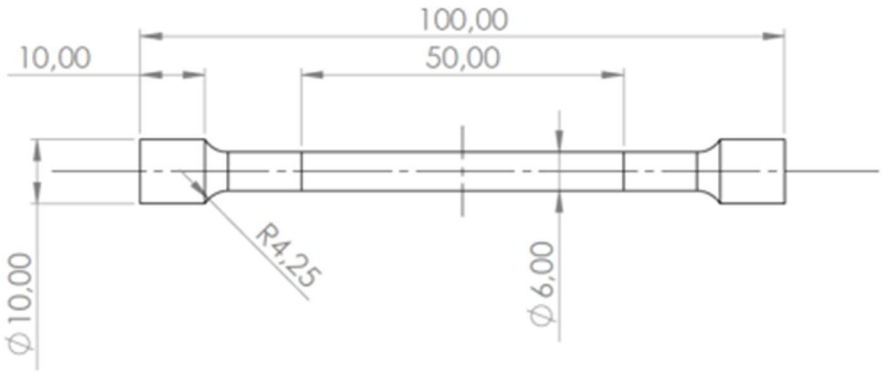

Figure 3.4 Tensile specimen dimensions

3.7. Deposition Parameters and Procedure for Part Construction

As mentioned in section 3.3, the first stage of this work was carried out in order to determine the optimal parameters for part building. After finishing this testing stage, analyzing and evaluating the resulting depositions led to the selection of the parameters to be used when building the proposed part.

This part was designed with challenge in mind rather than actual functionality, meaning that a set of somewhat challenging geometries for WAAM processing were selected and combined into a single part in order to determine the best strategies and process parameters that would lead to a successful build of these geometries using this material.

As referred in section 2.4, the deposition of the parts was carried out using two different software's, PowerMill, from Autodesk and a WAAM Software developed by Cranfield University, WAAMPlanner. Although both software's have 3D modelling capabilities, the 3D model of the part (see Figure 3.5) was created with SolidWorks from SolidWorks Corp.

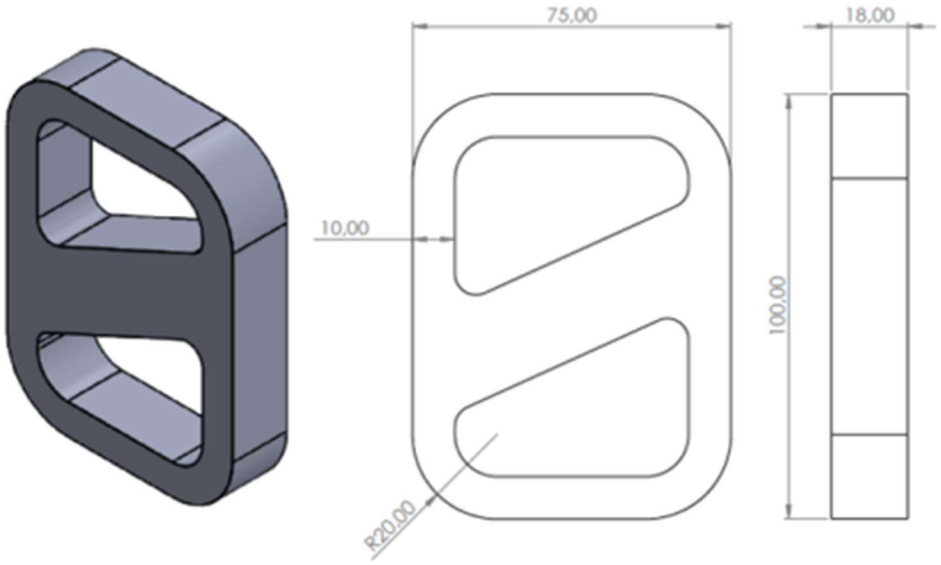

Figure 3.5 3D model of the deposited part and technical drawing

This part possesses thin walls, 90º angle corners and a middle section that intersects the outer section at an angle, presenting thus three challenges to overcome and achieve a successful build.

As mentioned in section 3.3, two sets of experiments were tested. For the first set two building strategies were employed (see Figure 3.6). In the first strategy, the outer section of the part was deposited with an oscillating motion while in the second one the same outer layer was deposited with a single bead linear deposition. In both strategies the middle section was produced with an oscillation motion.

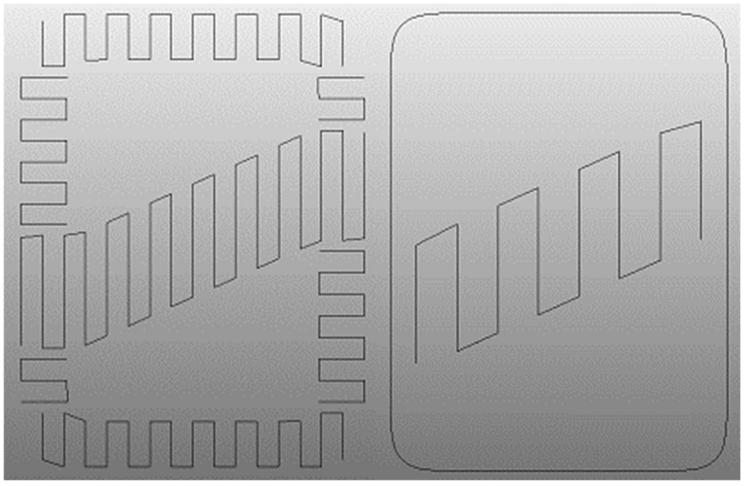

Figure 3.6 Strategies employed in the PowerMill Additive part deposition study

These strategies were created using Autodesk's PowerMill additive plugin and its depositions are evaluated in section 4.3.1.

In Figure 3.7 the main interface of PowerMill is presented. A 3D model of the part can be seen in the center as well as a representation of the different motions of the toolpath. The ArcOn movements, that corresponds to the situation where material is being deposited, are displayed in yellow and the ArcOff movements, which corresponds to the case where the arc is turned off and the tool is moved into position, are displayed in purple. In order to create a strategy for deposition the part must be oriented in a way where the tool axis is coincident with the Z-axis. Afterwards the model must be divided in levels, defining a base level and one or more building levels that depend on the geometry of the part.

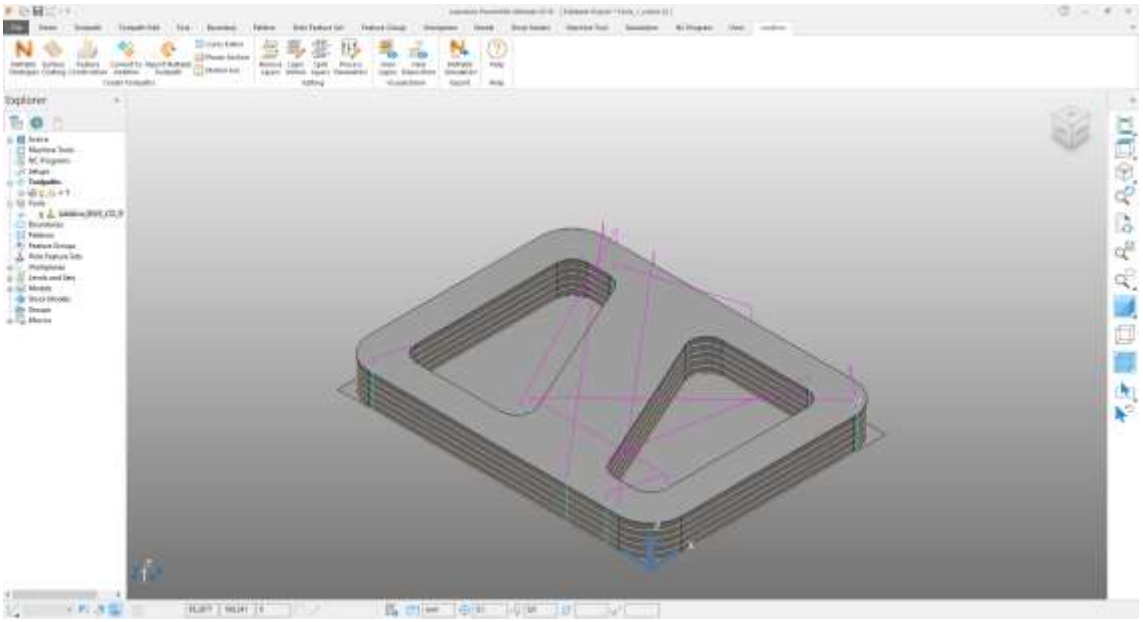

Figure 3.7 PowerMill interface

Figure 3.8 shows the deposition strategy creation window, and the different strategies available on PowerMill.

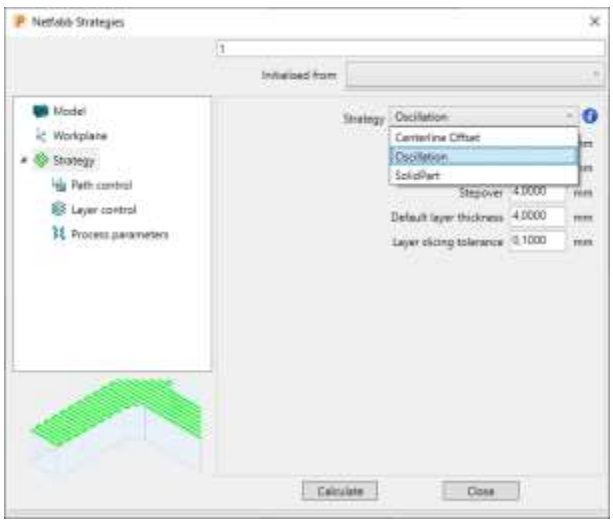

Figure 3.8 PowerMill building strategy creator interface – Strategy selection

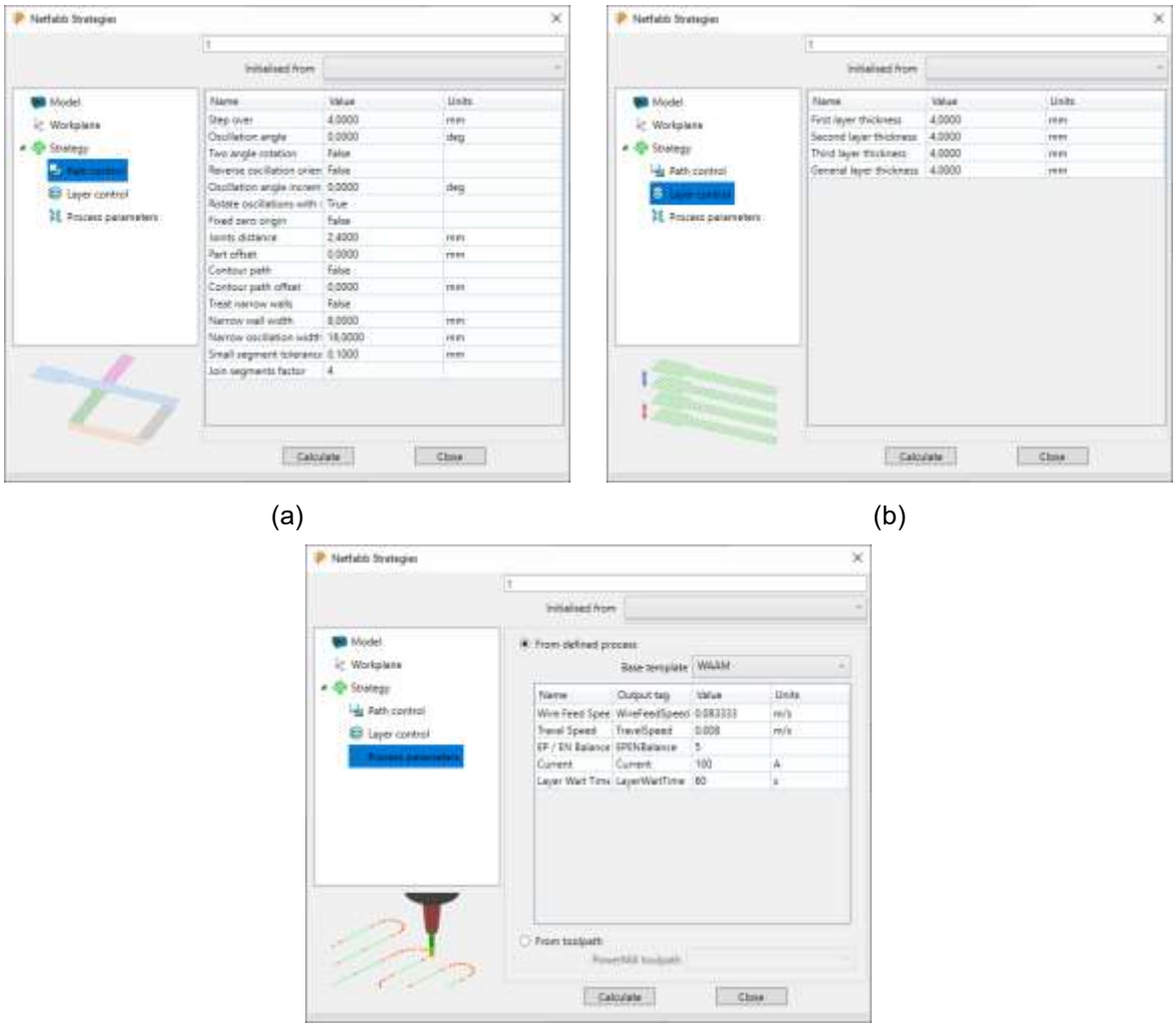

Figure 3.9 PowerMill building strategy creator interface - Process control: (a) Path control, (b) Layer control, (c) Process parameters

For the second set of experiments, a beta version of Cranfield's WAAM Software, WAAMPlanner, which only allows the use of an oscillation strategy at the moment, was used to produce the part. The main advantage of this software over PowerMill is the degree of control it provides over the sectioning of the part and the fine tuning of process parameters by defining custom zones. Figure 3.10 shows how the part was sectioned and the employed deposition path.

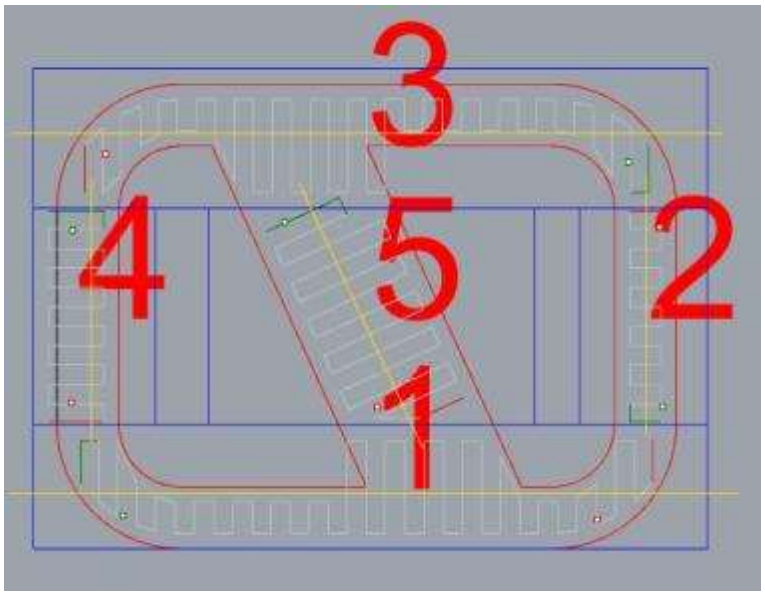

Figure 3.10 Strategy employed with WAAMPlanner

This software makes use of Rhinoceros and Grasshopper. The first is used to present the 3D CAD model, either created in Rhinoceros or imported from other 3D modelling software, the different layers of the part and the deposition paths. Grasshopper is used to define the process parameters, layer and path control and to generate the toolpath code files to be uploaded into the robot in order to deposit the part. Figure 3.11 shows the main interface of Rhinoceros.

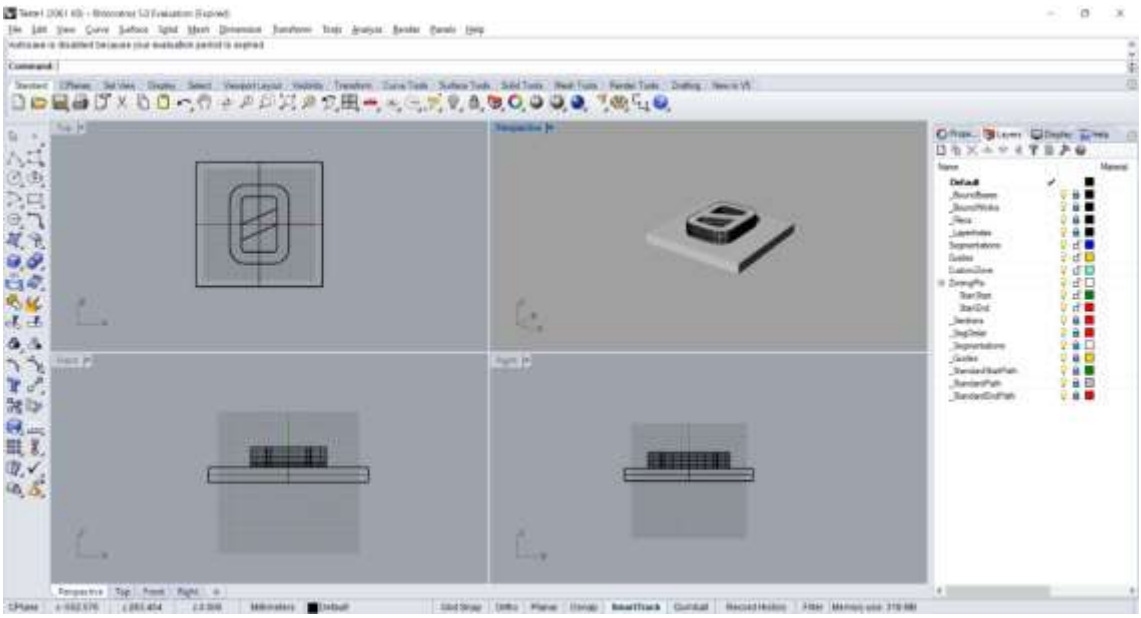

Figure 3.11 Main interface of the Rhinoceros software

In the center three orthogonal views of the model and a perspective are displayed, allowing the user to manipulate and view the model from various angles. On the right side there are five layers of the file that the user must manipulate to generate a strategy (on this instance “layers” is a designation that Rhinoceros uses and should not be confused with the layers of the deposition process). These five layers, and their function are, in order, the following:

- Segmentations – this allows the user to partition the part according to his needs, by drawing a dark blue box around the segment of the part. After doing so, a number is automatically assigned to each partition, which will later be used to define the order of segmentation deposition;
- Guides – defines the direction of the oscillation path, which will be perpendicular to yellow drawn line;
- ZoningPts – two points that define where the torch starts welding, StanStart, defined by a green point, and where the torch stops, StanEnd, defined by a red point;
- CustomZone – allows the user to set a zone where the process parameters are different from the main process parameters. This zone is defined by a light blue box.

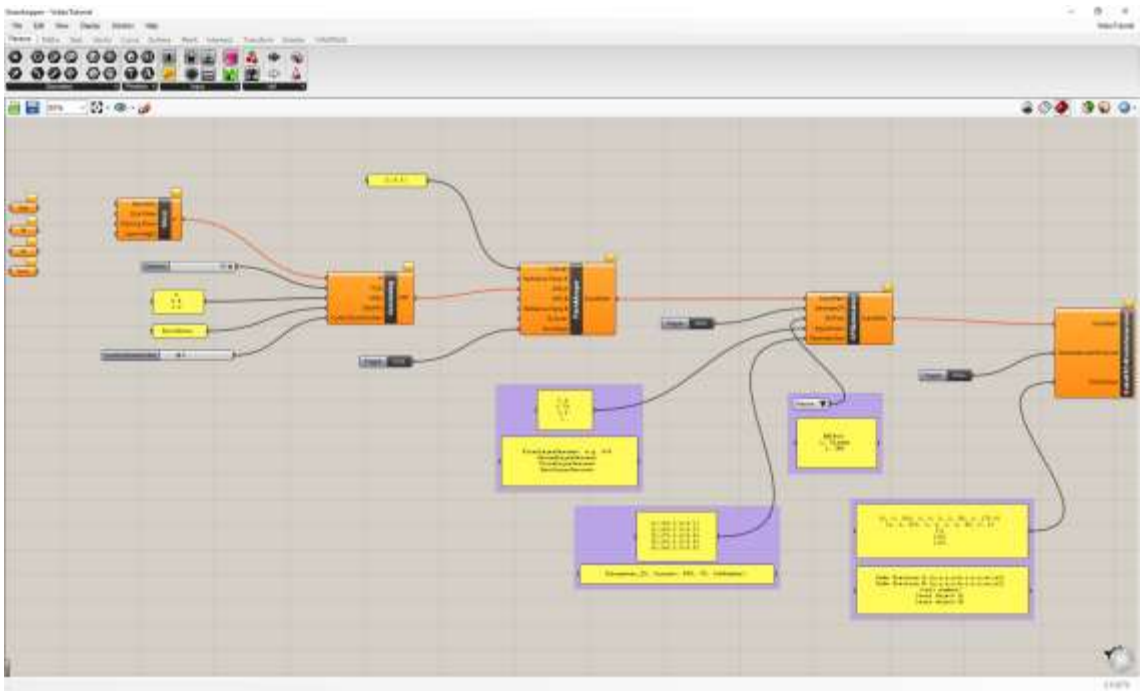

Figure 3.12 Main interface of the Grasshopper plugin for Rhinoceros

Figure 3.12 shows the main interface of Grasshopper, which is composed by five main blocks. An explanation on the functions of these blocks is provided in Appendix B.

4. Results and Analysis

This chapter presents the results associated to the different tests described in chapter 3. Metallographic analysis, hardness tests and tensile tests will also be discussed

Based on the results obtained a final part was produced.

4.1. Deposition parameters

As mentioned in section 3.3 two sets of deposition tests were carried out. In this subsection the resulting depositions will be analyzed.

4.1.1. First set of experiments

Figure 4.1 shows the results of the first set of depositions, which consists of sixteen linear depositions.

Figure 4.1 Results of first set of depositions

Table 4.1 shows the parameters that were used in the first stage of depositions.

Table 4.1 Process parameters for the first set of depositions

Experiments	**Parameters**				
	CTWD [mm]	**SGFR [L/min]**	**WFS [m/min]**	**WFS/TS**	**TS [m/min]**
1	15	18	3	10	0.30
2				15	0.20
3				20	0.15
4				25	0.12
5			4	10	0.40
6				15	0.27
7				20	0.20
8				25	0.16
9			5	10	0.50
10				15	0.33
11				20	0.25
12				25	0.20
13			6	10	0.60
14				15	0.40
15				20	0.30
16				25	0.24

Sixteen experiments were performed, four for each value of WFS allowed by the welding machine controller, ranging from 3 to 6 m/min, and defined ratios of WFS/TS, ranging from 10 to 25. The CTWD and SGFR were both kept constant at 15 mm and 18 L/min, respectively.

After depositing, each experiment was evaluated by visual inspection and sorted into acceptable and unacceptable categories. The results of this inspections are presented in Figure 4.2.

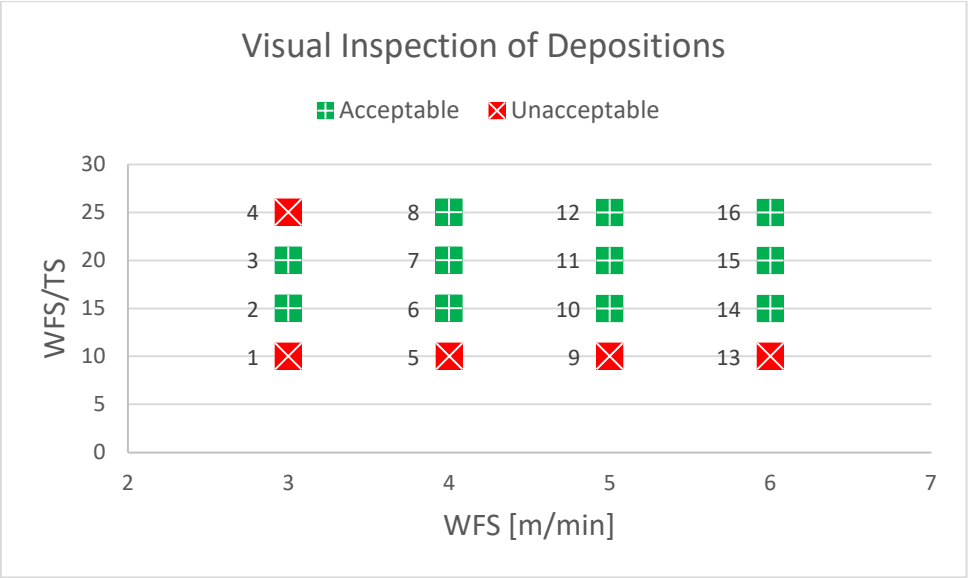

Figure 4.2 Visual inspection evaluation of first set of depositions

From Figure 4.2 it can be seen that, with the exception of the experiments pertaining to WFS/TS ratios of 10 (1, 5, 9, 13) and experiment 4, all other experiments are classified as acceptable. Acceptable depositions are those which do not show any glaring defects, such as excess or lack of material in any given area or deviations in their measurements visible to the naked eye. Experiences 1, 5, 9 and 13 were classified as unacceptable because they do not provide depositions with enough height due to their high TS. Experiment 4 was classified as unacceptable because the extremities of the bead showed a significant drop in height due to the low WFS used which could not provide enough material to fill that part of the weld bead.

Each bead was also measured with the use of calipers. Taking measures from three points along the part, two near the extremities and one in the center, an average of these dimensions and the percent deviation were calculated. Table 4.2 presents the measured dimensions of width and height for each experiment, the average of these dimensions along the part and the percentage of deviation of these dimensions from the average. Figure 4.3 shows a graphical comparison between the average height and width for each experiment.

Dimension	Experiments															
	1	2	3	4	5	6	7	8	9	10	11	12	13	14	15	16
Width [mm]	5,55	5,82	6,85	7,56	5,05	7,23	7,64	8,50	5,66	7,46	8,78	9,88	6,35	7,62	8,81	10,02
	4,58	5,79	6,93	7,81	5,29	6,77	7,95	8,56	5,96	7,32	8,67	10,35	6,28	7,41	9,05	9,73
	4,57	6,02	6,97	6,88	5,22	6,67	7,60	8,56	5,95	7,69	8,53	10,31	6,38	7,61	8,41	9,91
Average Width [mm]	4,90	5,88	6,92	7,42	5,19	6,89	7,73	8,54	5,86	7,49	8,66	10,18	6,34	7,55	8,76	9,89
% of Deviation	43%	10%	4%	36%	9%	23%	15%	3%	13%	13%	9%	20%	4%	9%	23%	10%
Height [mm]	13,10	16,37	17,54	18,49	10,82	13,27	13,83	15,20	9,39	11,26	12,74	13,25	9,18	10,93	12,93	13,93
	14,20	17,64	19,05	19,81	11,34	14,28	14,30	15,28	10,06	12,38	13,35	14,25	9,35	11,42	13,47	14,52
	14,44	17,35	18,75	19,20	11,76	14,05	14,06	15,11	9,96	12,56	13,25	13,94	9,81	11,26	13,67	13,74
Average Height [mm]	13,91	17,12	18,45	19,17	11,31	13,87	14,06	15,20	9,80	12,07	13,11	13,81	9,45	11,20	13,36	14,06
% of Deviation	54%	50%	60%	45%	32%	40%	16%	6%	28%	54%	25%	38%	24%	18%	28%	30%

Table 4.2 Dimensions of the first set of experiments

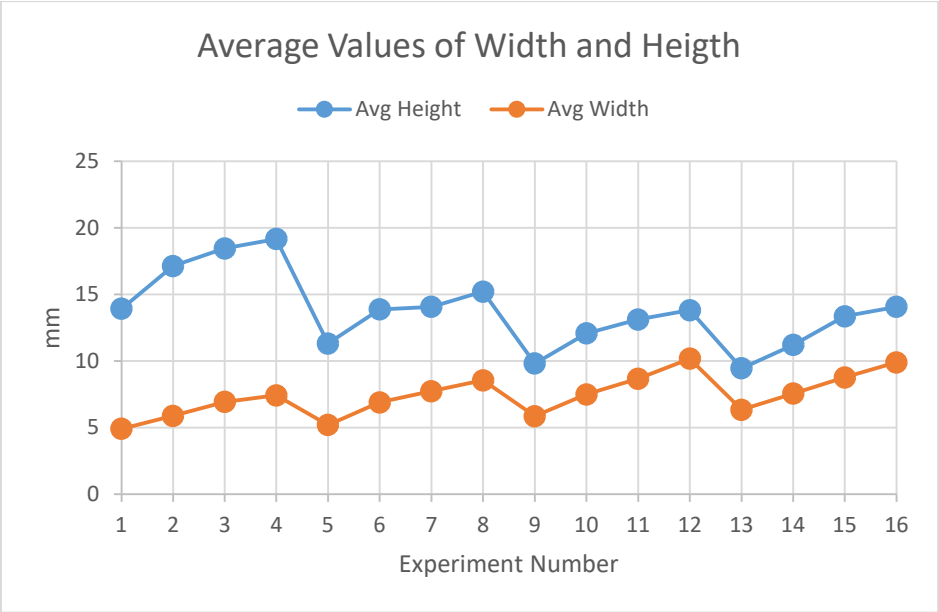

Figure 4.3 Average values of width and height for each experiment

Observing Figure 4.1 in combination with Table 4.2 and Figure 4.3 it can be seen that the width of the deposits, for the same value of WFS, increases with the WFS/TS ratio. This is expected behavior since increasing WFS/TS means reducing the TS of the torch, introducing more material into the melt pool. For the same reason, increasing the WFS also leads to larger bead width for the same WFS/TS ratio, although in a smaller magnitude. The average height of each bead increases when the WFS/TS ratio is increased and the WFS is kept constant, as expected, also due to more material being deposited per unit of length which allows for the height to build up quicker.

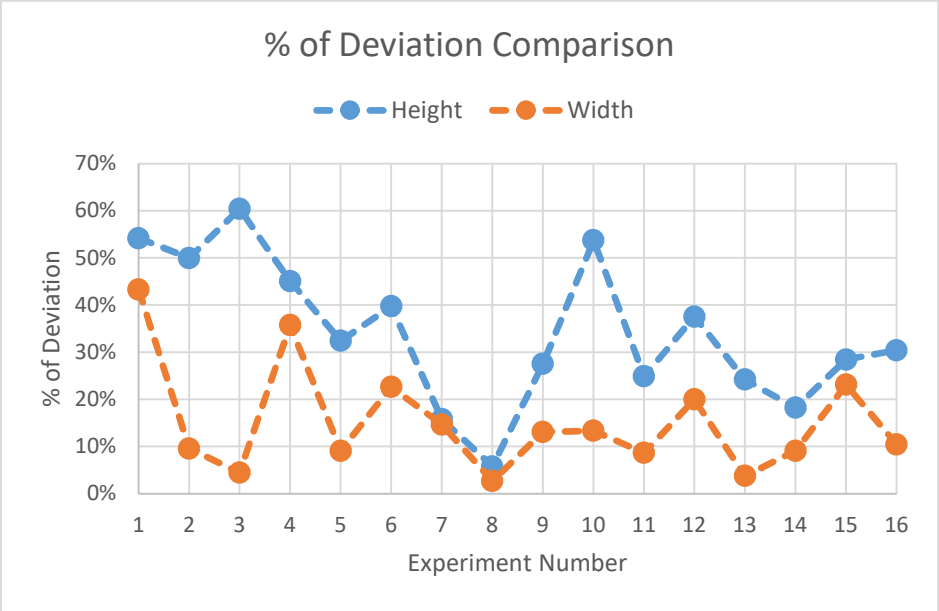

Figure 4.4 Comparison of % of deviation for height and width for each experiment

4.1.2. Second set of experiments

As referred in section 3.7, a second set of experiments were carried out with the purpose of determining the best parameters that would allow for defect free depositions when employing an oscillation strategy using Cranfield's University WAAM Software, WAAMPlanner. These experiments are described and analyzed on this subsection.

Figure 4.5 shows the results of the second set of deposition parameters study, with the relevant depositions numbered from 1 to 9.

Figure 4.5 Experimental results of second set of depositions

On this study a range of WFS was set between 3 m/min and 6 m/min, as well as a range of WFS/TS between 10 and 20. The CTWD was set at 15 mm and a SGFR was set at 18 L/min. Table 4.3 presents the parameters used on this study for each experiment and Figure 4.6 shows the appreciation of the visual inspections.

Table 4.3 Process parameters for the second set of depositions

Experiments	Parameters				
	CTWD [mm]	SGFR [L/min]	WFS [m/min]	WFS/TS	TS [m/min]
1	15	18	3	10	0.30
2				15	0.20
3				20	0.15
4			4	10	0.40
5				15	0.27
6				20	0.20
7			5	10	0.50
8				15	0.33
9			6	10	0.60

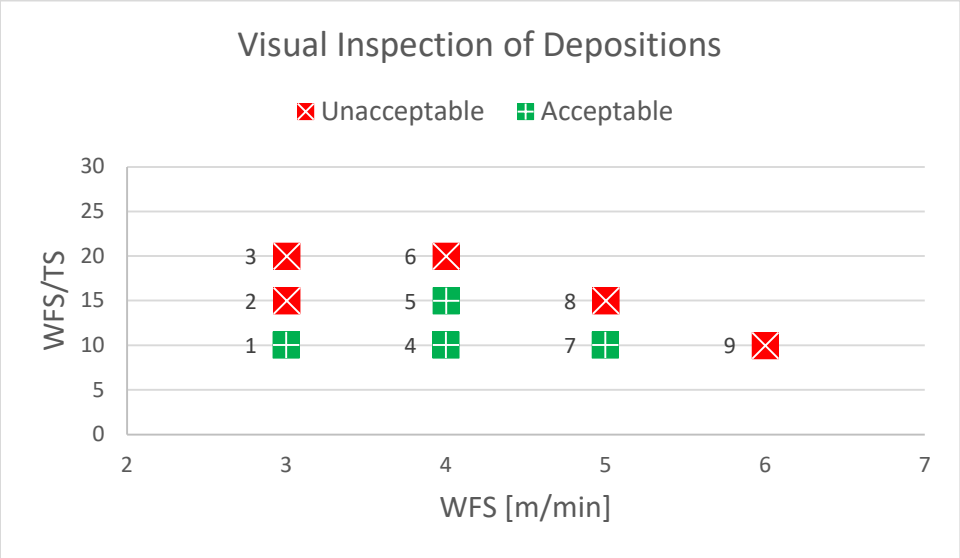

Figure 4.6 Visual inspection evaluation of second set of depositions

From Figure 4.6 it can be seen that experiments 1, 4, 5 and 7 are classified as acceptable, following the same criteria from section 4.1.1. The remaining experiments present, at least, one of such defects, which earns them the classification of unacceptable and excludes them from the list of parameters to be tested during part deposition.

Table 4.4 presents the measured dimensions of width and height for each experiment, the average of these dimensions along the part and the percentage of deviation of these dimensions from the average.

Table 4.4 Dimensions of the second set of experiments

Dimensions	Experiments								
	1	2	3	4	5	6	7	8	9
Width [mm]	18.10	18.25	23.81	17.26	20.72	24.03	20.37	15.43	24.24
	17.75	18.15	24.47	17.98	21.39	22.17	18.86	13.71	26.10
	18.15	18.4	23.93	17.27	21.53	22.05	19.39	16.15	24.52
Average Width [mm]	18.00	18.27	24.07	17.50	21.21	22.75	19.54	15.10	24.95
% of Deviation	17%	9%	27%	32%	33%	85%	55%	92%	76%
Height [mm]	21.48	16.11	19.72	24.36	18.62	17.01	13.76	15.17	7.92
	22.18	17.72	21.48	25.30	19.87	17.7	13.94	15.39	8.22
	21.98	17.15	20.88	25.16	19.51	16.54	13.48	12.63	8.02
Average Height [mm]	21.88	16.99	20.69	24.94	19.33	17.08	13.73	14.40	8.05
% of Deviation	27%	59%	65%	39%	48%	41%	16%	118%	11%

The values for smallest and largest percentage of deviation are highlighted in green and red, respectively. It can be seen that experiment 8 has the largest deviation both in width and thickness, automatically excluding it from consideration when selecting parameters for part construction. Although experiment 2 has the smallest percentage of deviation for width and experiment 9 has the smallest percentage of deviation for thickness, they both show high values in percentage of deviation for height and width, respectively, which makes them not ideal in a list of possible candidates for the final part deposition. Figure 4.7 shows a comparison of percentage of deviation for both width and height for each experiment.

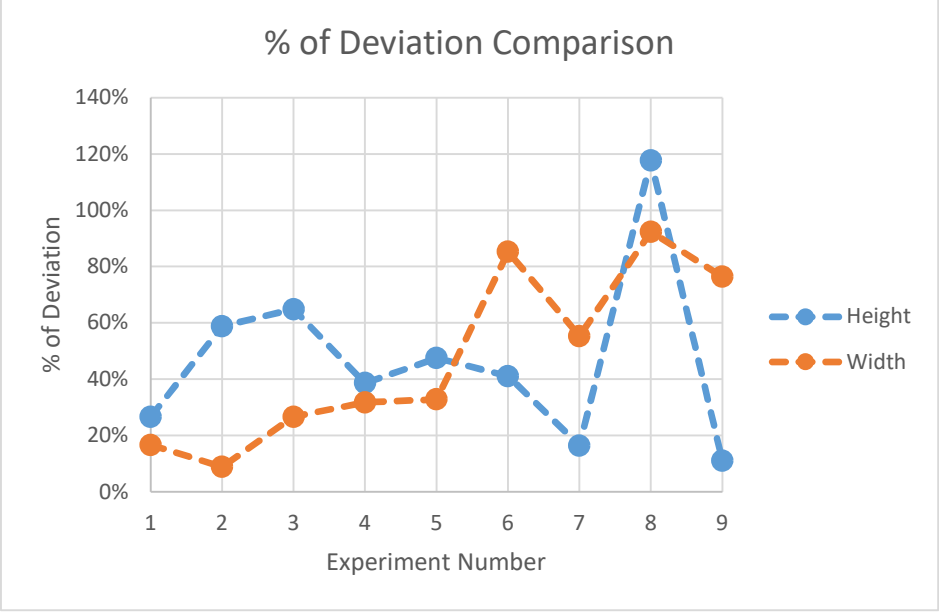

Figure 4.7 Percentage of Deviation comparison by experiment

It can be seen from Figure 4.7 that experiments 1, 4 and 5 offer the best balance between height and width, with experiment 1 showing the smallest values of percentage of deviation, making them candidates for the final part deposition.

This preliminary deposition work allowed for the determination of a set of parameters that yielded depositions that were, not only regular, but also had adequate mechanical properties and microstructures, which in turn allowed for the production of parts that met the required objectives.

4.2. Material Characterization

In the following subsection results from the performed material characterization tests are presented.

4.2.1. Metallographic Analysis

In the following subsections a macroscopic and microscopic analysis will be performed.

4.2.1.1. Macroscopic Analysis

In Figure 4.8 the microstructure of a section of a wall is presented. In the same figure it can be observed the gradient of microstructure along the wall, in which can be distinguished the first layers (Figure 4.8 – (a)), HAZ (Figure 4.8 – (b)), start of the columnar region (Figure 4.8 – (c)) and the last layers (Figure 4.8 – (d)), where it is observed a well-known grain morphology of AM parts, a columnar region aligned along the buildup direction, following the heat flow direction towards the surface of each bead.

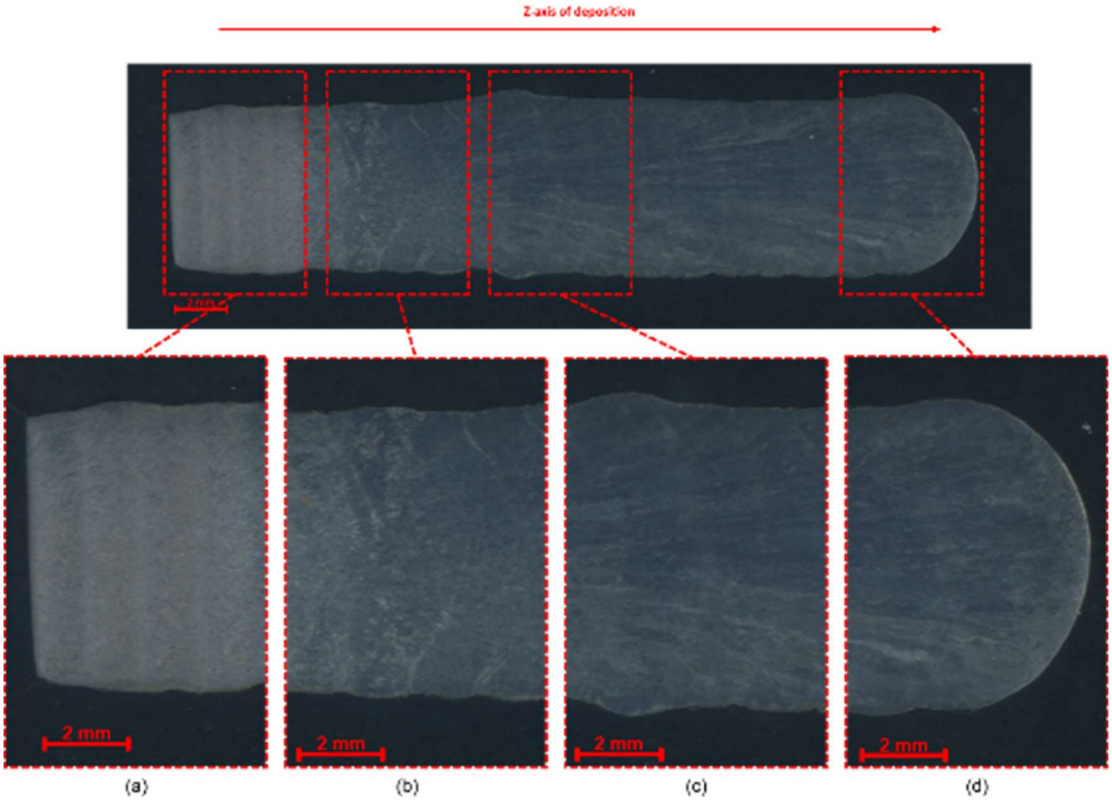

Figure 4.8 Macrostructure of a section of a deposited wall

4.2.1.2. Microscopic Analysis

In this subsection a microscopic analysis is presented. During microscopic observation of the sample none of the common welding defects, such as cracks, porosity or lack of fusion were detected. Being a martensitic grade steel, AISI 410 is prone to cold cracking, a defect that occurs when a martensitic microstructure, trapped hydrogen in the heat-affected zone and residual stresses are all present simultaneously. Multiple methods to mitigate this defect are available in welding literature, and many, like pre and post heating, are intuitively applied in WAAM due to the characteristics of the process. As mentioned in section 3.1, AISI 410 is considered a supermartensitic stainless steel, and, due to its low carbon content, it forms a "soft" low-carbon martensite which increases its resistance to hydrogen induced cracking when compared to standard martensite.

The appearance of martensite observed microscopically changes according to the percentage of carbon equivalent (C_{eq}), which can be determined by equation 4.1. This equation combines the effect of the various alloying elements that affect the hardenability of the material.

$$C_{eq} = C + \frac{Si}{25} + \frac{Mn + Cu}{16} + \frac{Cr + Ni}{20} + \frac{Mo}{40} + \frac{V}{15} \tag{4.1}$$

It has been determined that, for $\%C_{eq}$ between 0 and 0,6, lath martensite is formed (Figure 4.9 – (a)), while for $\%C_{eq}$ higher than 1, plate martensite is formed (Figure 4.9 – (b)), with a mixture of these two being present when intermediate values of $\%C_{eq}$ are verified (Figure 4.9 – (c)). While pure lath martensite and mixed lath + plate martensite are not immediately discernible when observed at a microscope, plate martensite has a distinct appearance due to the fact that white regions surround the plates, making them stand out. These white regions are grains of austenite that did not underwent transformation, called retained austenite. If the plates do not stand out then the sample contains residual amounts or no austenite at all [75].

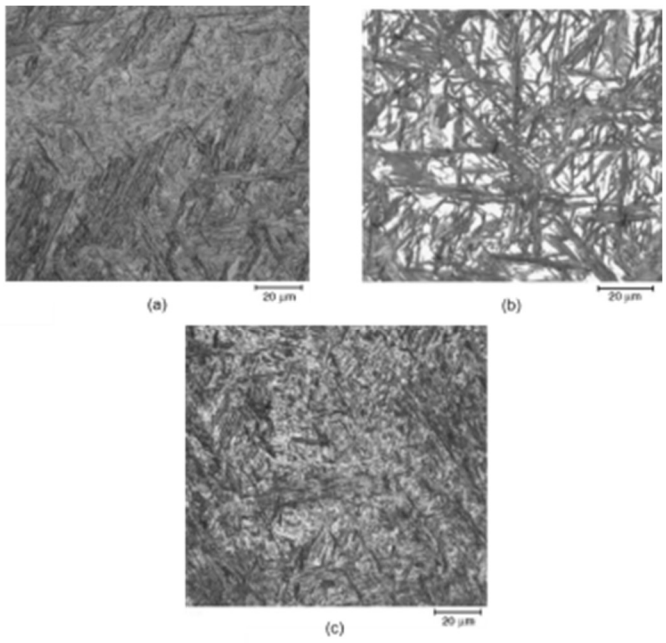

Figure 4.9 Different appearances of martensite according to $\%C_{eq}$ [75]

Figure 4.10 shows the microstructure in the bottom portion of the sample.

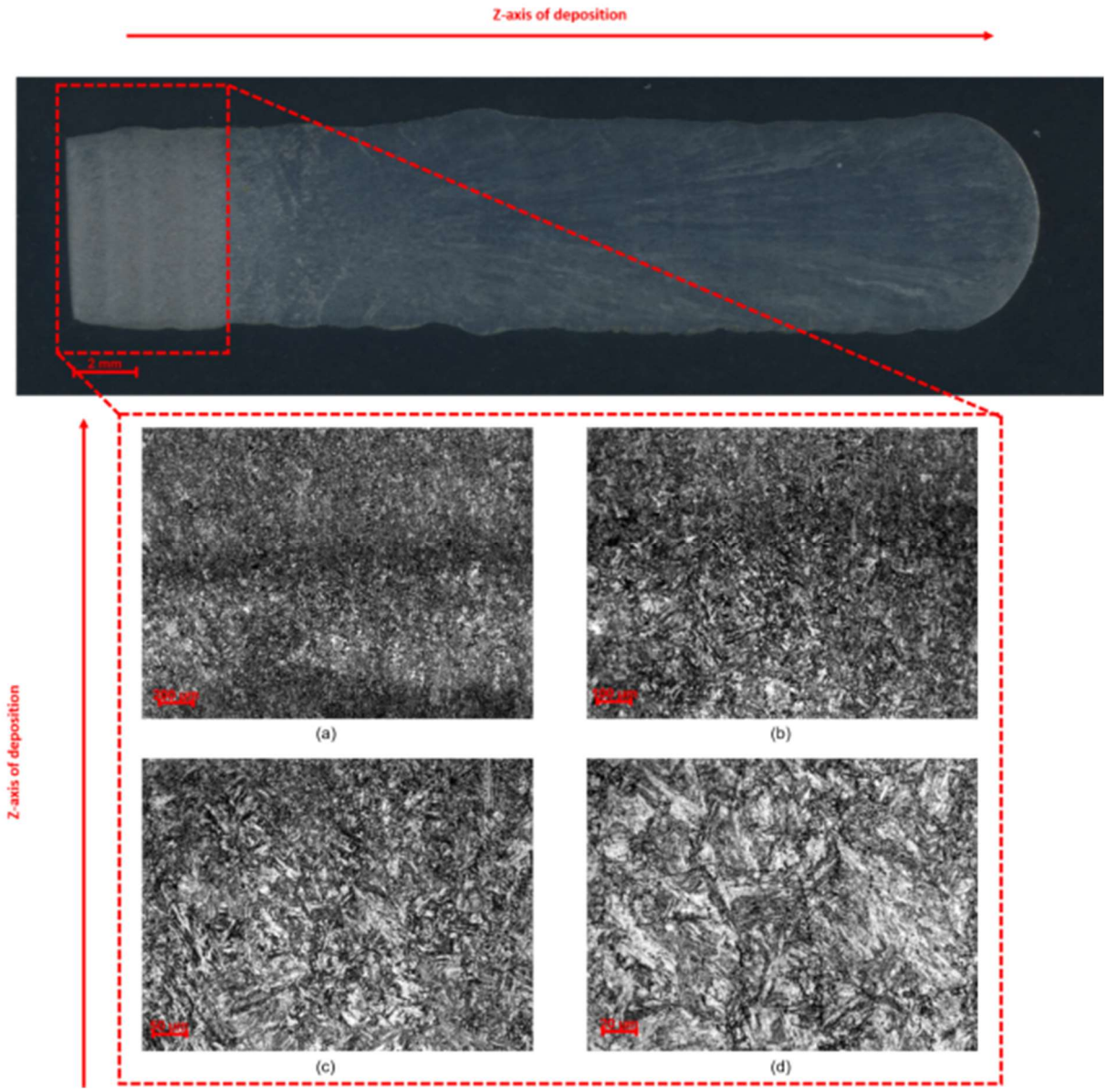

Figure 4.10 Microstructure in the bottom portion of the sample

Observing Figure 4.10 a nearly fully martensitic microstructure is visible. With 0,91 of $\%C_{eq}$, a mixture of lath and plate martensite was expected in accordance to what was previously explained in this section and, comparing Figure 4.9 – (c) with Figure 4.10 – (d), many similarities can be found between them. Some amounts of retained austenite can also be discerned, which, being softer than martensite, leads to a decrease in hardness and an increase in ductility.

Figure 4.11 shows the microstructure in the depicted zone.

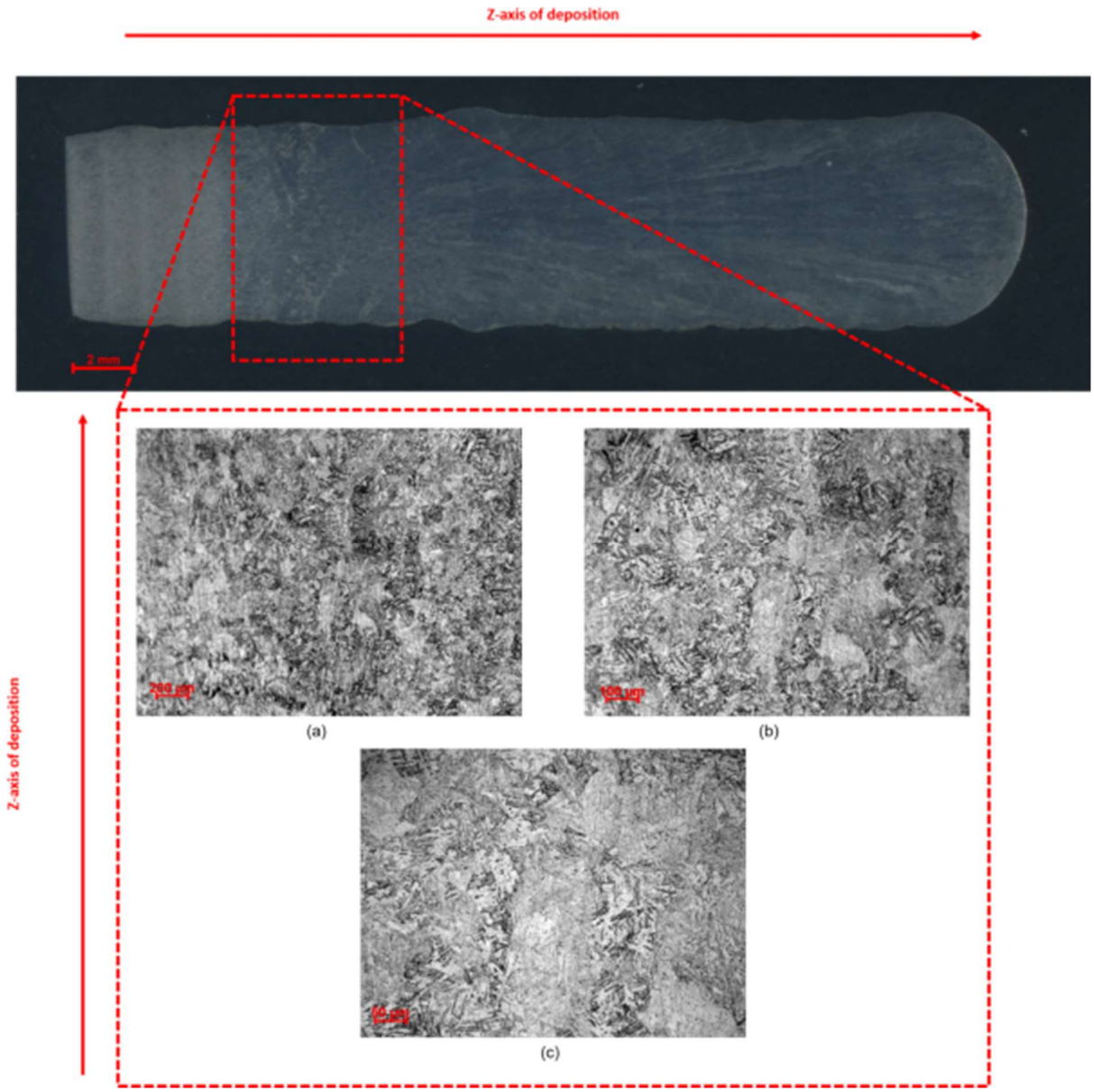

Figure 4.11 Microstructure in the middle portion of the sample

Figure 4.11 shows a mixture of tempered and freshly formed martensite. The martensite present in these section of the sample shows a finer microstructure than the one present in Figure 4.10. Carbides can also be observed, showing as small round dots. Grain size also shows an increase in dimension due to the additional thermal cycles, with a further increase expected closer to the top of the sample.

Figure 4.12 shows the microstructure near the top of the sample.

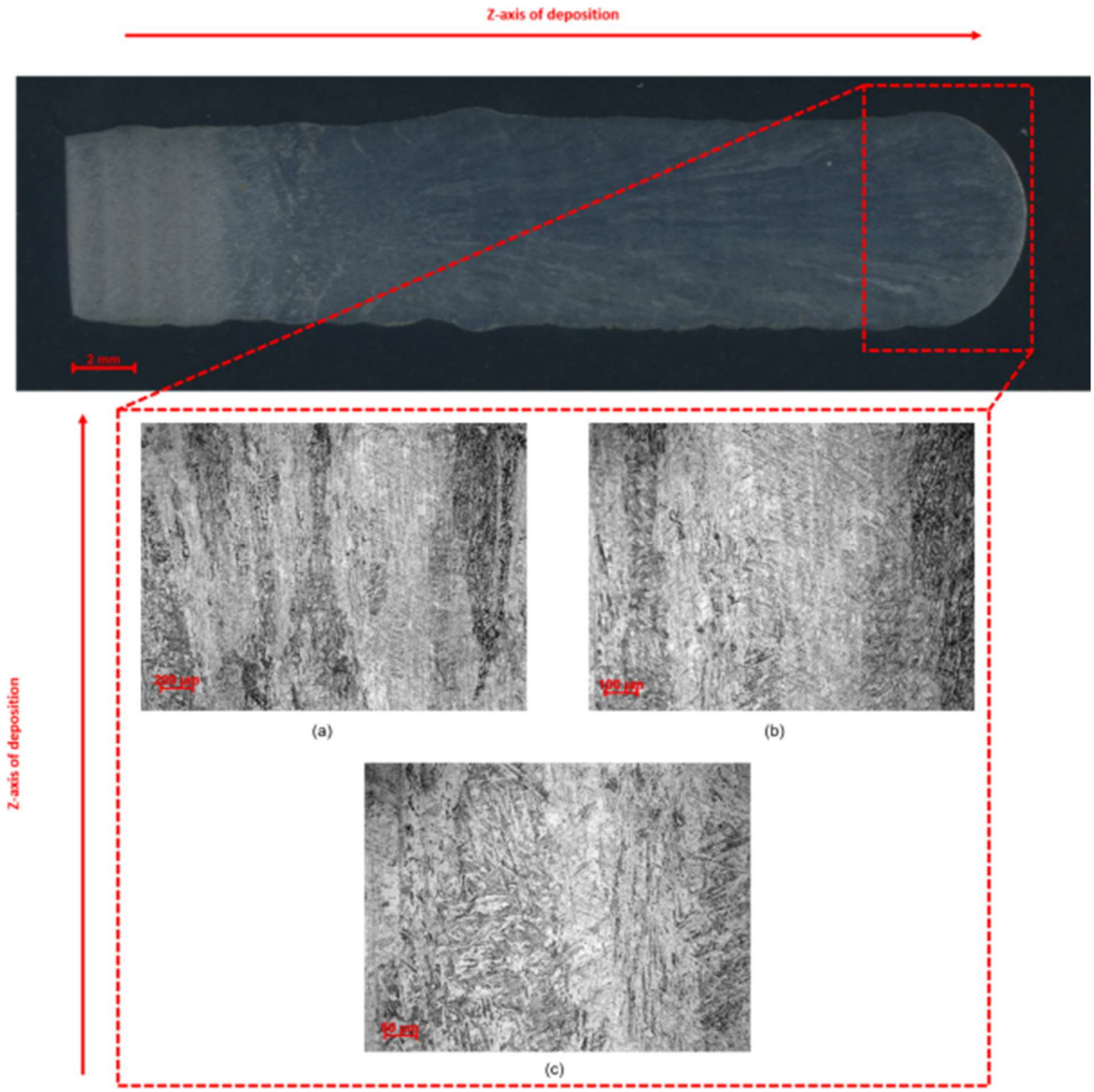

Figure 4.12 Microstructure near the top of the sample

Figure 4.12 shows regions with column shaped microstructure and fine martensite microstructures. This column shaped microstructure follows the direction of the heat flow towards the top of the sample. These were probably austenite columnar grains that were not modified in a significant manner by the martensitic transformation during cooling. Another possible explanation is that, in some regions, the heat of the deposition of new layers raised the temperature to the austenitic region and, as they cooled and transformed back into fresh martensite, the columnar microstructure remained [52]. Carbides are also visible in these micrographs. Like expected, successive thermal cycles increased grain size even further when compared with the previous analyzed section.

4.2.2. Hardness Tests

On this subsection the values gathered in the hardness tests are presented as well as their correlation with UTS and YS. Table 4.5 shows the Vickers hardness values for the analyzed samples and the values for UTS and YS calculated from the expressions presented in section 3.5.

Table 4.5 Values for Vickers Hardness and predicted UTS and YS calculated from Equation 3.1 and Equation 3.2

Variables	Samples				
	1	2	3	4	5
Vickers Hardness [HV]	390	316	331	357	364
	433	441	400	364	412
	444	444	414	355	424
	394	426	352	388	414
	425	433	395	392	399
	406	406	445	390	422
	408	404	429	382	378
	405	421	437	377	378
	410	418	430	347	411
	400	414	418	372	401
Average Vickers Hardness [HV]	412	412	405	372	400
Ultimate Tensile Strength [MPa]	1437	1440	1413	1291	1395
Average Ultimate Tensile Strength [MPa]	1395				
Yield Strength [MPa]	1093	1095	1074	980	1061
Average Yield Strength [MPa]	1061				

Figure 4.13 shows the correlation between Vickers Hardness and both UTS and YS.

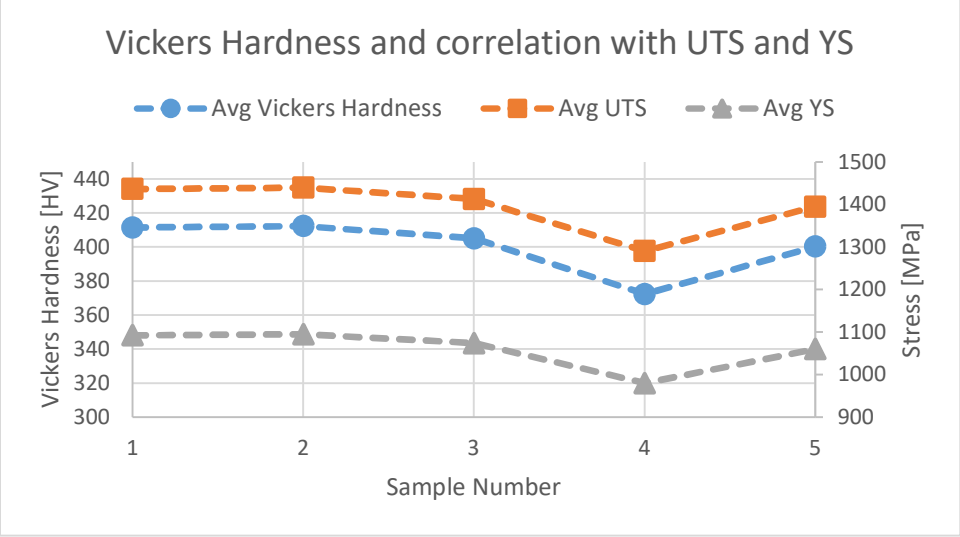

Figure 4.13 Correlation of Vickers Hardness with UTS and YS

The average values found for Vickers Hardness of the AISI 410 WAAM samples were between 372 HV and 412 HV, lower than the value of 450 HV obtained for the weld metal in the “as welded” condition, determined in [76], but in line with the values obtained by *Amrei et al.* [52] for a multipass welding of this material. This is related with the constant reheating of the sample with every successive layer, which leads to coarser grain size, verified in section 4.2.1.2, which in turn leads to a decrease in hardness. The hardness was found to be independent of the process parameters used in the manufacturing of the sample.

The average values for UTS and YS were 1394,99 MPa and 1060,62 MPa, respectively, which are superior to the values for UTS and YS supplied by the manufacturer, (1050 MPa and 860 MPa, respectively for the “as welded” condition), and outside the standard errors defined for these correlations.

4.2.3. Tensile Tests

The tensile tests performed for both the transversal (perpendicular to the direction of deposition) and longitudinal (parallel to the direction of deposition) samples are presented in Table 4.6. Samples T1 to T3 pertain to the transversal tensile specimens while samples L1 and L2 pertain to longitudinal tensile specimens. For comparison, data from the manufacturer regarding the typical tensile properties of this material as welded is also presented.

Table 4.6 Yield Strength, Ultimate Tensile Strength and Strain at fracture, determined by tensile testing

	Tensile Properties		
Samples	**YS 0,2% [MPa]**	**UTS [MPa]**	**Strain**
T1	970	1226,44	0.06
T2	941	1235,12	0.07
T3	949	1223,75	0.06
L1	887	1091,89	0.10
L2	842	1122,42	0.08
As welded	860	1060	0.13

Figure 4.14 shows the true stress-strain curve until necking of samples T3 and L1.

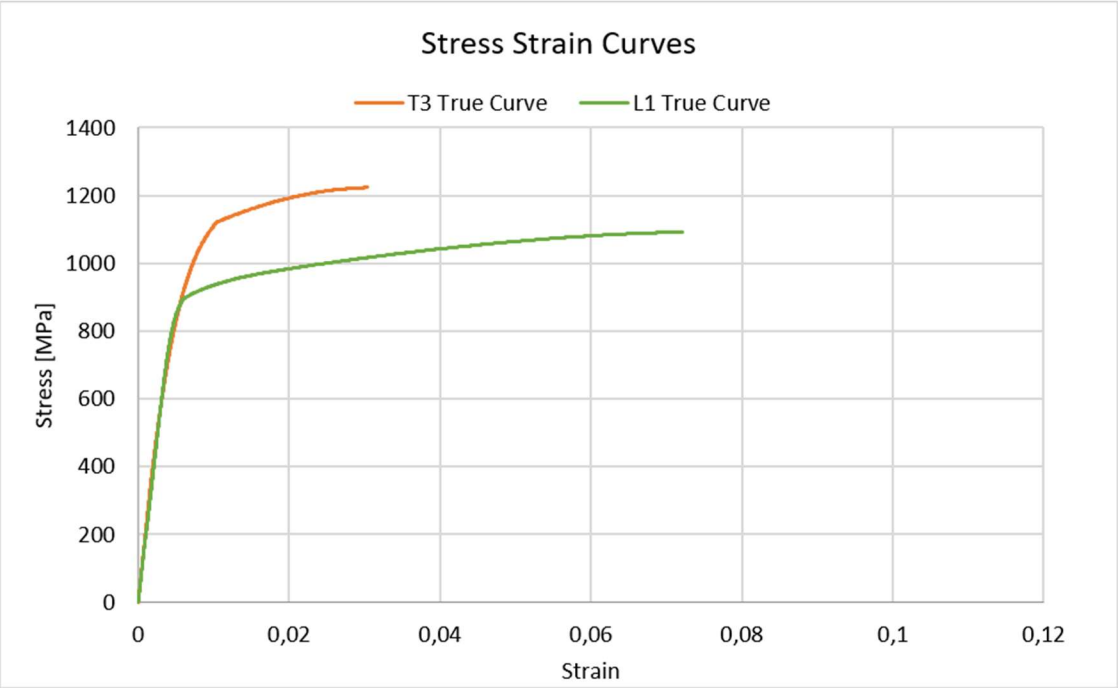

Figure 4.14 True stress-strain curves of samples T3 and L1

From Table 4.6 and Figure 4.14 we can observe that transversal samples offer a higher degree of tensile strength than longitudinal samples (1235,12 MPa vs 1122,42 MPa), while longitudinal samples offer a considerable greater degree of ductility (0,10 vs 0,07). This difference suggests that thermal history has a significant impact on material properties. As expected, longitudinal samples show a closer agreement with manufacturer tensile properties since the specimens didn't span such a wide range of thermal cycles when compared to transversal samples, leaving them closer to the "as welded" condition. The lower ductility on the transversal samples could also suggest lack of fusion or other defects between layers.

Comparing the values obtained from tensile testing with the ones obtained from hardness correlations we can observe that, although still outside the standard error for UTS, they show a closer relationship than when compared with the values supplied by the manufacturer.

4.2.4. Material characterization summary

Material characterization tests show that it is possible to process AISI 410 by WAAM while retaining the mechanical characteristics that make this material attractive.

In the metallographic analysis it was observed that the microstructure was composed almost entirely by martensite, with small amounts of retained austenite. Nevertheless, this microstructure was not uniform along the sample, with progressively coarser grain sizes along the height of the sample.

Hardness testing revealed average values between 372 HV and 412 HV, values in the range of what was observed by Amrei *et al.* [52], and characteristic of martensitic structures.

Tensile tests, performed in two different orientations, perpendicular (transversal samples) and parallel (longitudinal samples) to deposition direction, showed an anisotropy in tensile properties, in accordance with what was observed by Wang *et al.* [53] for H13 steel. Transversal samples showed greater strength, but lower ductility than longitudinal samples.

4.3. Part Deposition

One of the goals of this section is to test different software's to determine which one provides a greater degree of control over the deposition procedure and thus allows us to achieve better deposited parts. For that purpose, as mentioned in section 2.4 two software's, PowerMill Additive and WAAMPlanner were used to produce the part. In a first stage PowerMill Additve was used to deposit the part, using the parameters determined in the first study mentioned in section 4.1.1, but after unsatisfactory results obtained during this experiment, parts were made using WAAMPlanner with the second set of parameters determined and analyzed in section 4.1.2.

On this section the deposited parts using both software's are analyzed.

4.3.1. Depositions made with PowerMill Additive

The deposited part as well as the employed strategies used are described in section 3.7. Eight depositions were carried out (see Figure 4.15), with deposition 3 through 6 using a reduced version of the original part. This version of the part had its dimensions reduced by a third.

Figure 4.15 Experiments performed for the part deposition with PowerMill Additive

The parameters used in each deposition are presented in Table 4.7.

Table 4.7 Process parameters for the experiments with PowerMill Additive

Experiments	Parameters				
	CTWD [mm]	SGFR [L/min]	WFS [m/min]	Stepover [mm]	TS [m/min]
1	10	18	4	4.5	0.16
2				4.5	0.20
3				4.5	0.20
4				5.5	0.20
5				5.5	0.27
6				5	0.27
7				5	0.27
8				5	0.27

Figure 4.16 shows the result of the first experiment.

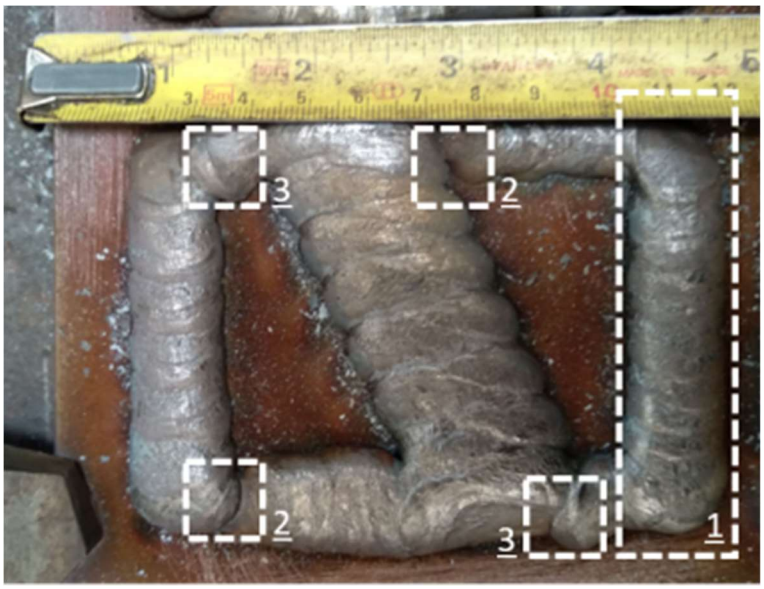

Figure 4.16 First experiment of part deposition with PowerMill Additive

A number of issues are immediately apparent. The shape is highly irregular, with severe variations in dimensions in the different segments of the part (Figure 4.16 – 1) as well as a deficient connection between them (Figure 4.16 – 2). The toolpath continuity also needs to be improved, since there are small segments that should be avoided because the process cannot guarantee high precision when depositing in such small segments (Figure 4.16 – 3).

Figure 4.17 shows the result of the second experiment.

Figure 4.17 Second experiment of part deposition with PowerMill Additive

In the second trial, although some slight improvements can be observed, with more regular segments of the part, the main issues from the first deposition remain.

Figure 4.18 shows the results of the third experiment. The top left corner (Figure 4.18 – 1) shows an irregular shape due to the starting position of the welding process being kept constant. In subsequent depositions, precautions were taken to ensure that the starting position was changed between each layer and that it wasn't overly close to the corners. The middle section of the part (Figure 4.18 – 2) also shows irregularities due to an inadequate stepover (4.5 mm) for the used parameters.

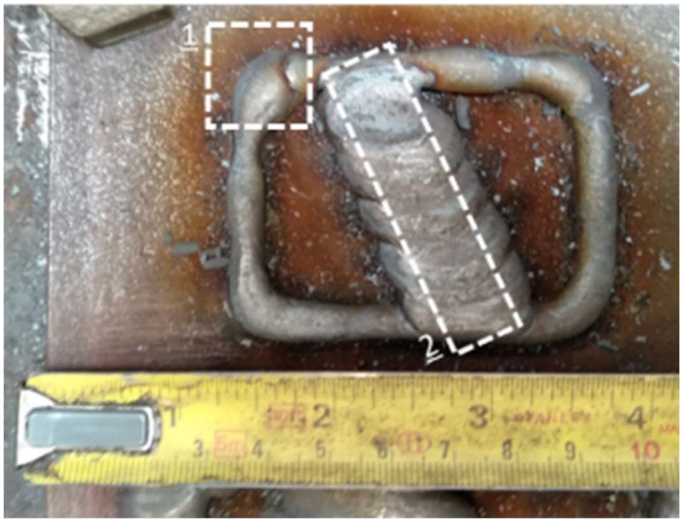

Figure 4.18 Third experiment of part deposition with PowerMill Additive

Figure 4.19 represents the result of the fourth experiment. In this experiment the previous parameters were kept with the exception of the stepover in the middle section, which was increased from 4.5 mm to 5.5 mm. As it turns out, this change led to a worse result than the one obtained from the previous

deposition, with a more irregular middle section (Figure 4.19 – 1) and also a worse connection with the outer perimeter of the part (Figure 4.19 – 2).

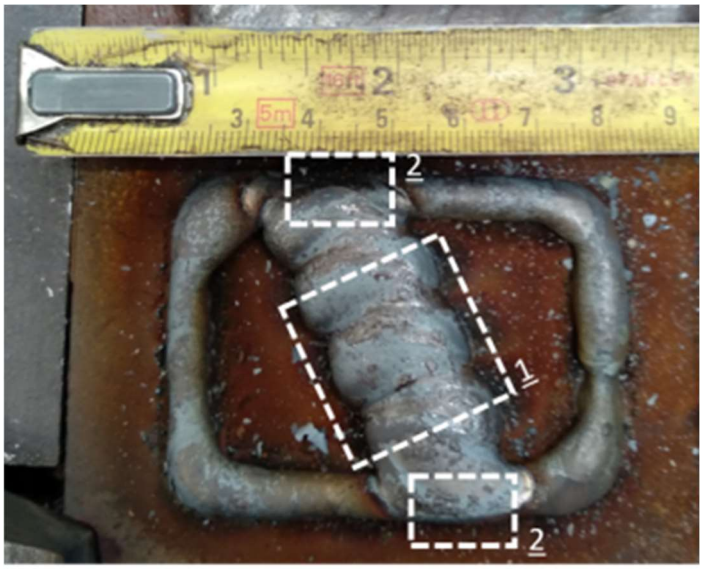

Figure 4.19 Fourth experiment of part deposition with PowerMill Additive

Figure 4.20 shows the results of the fifth experiment. An improvement can be seen with this deposition. The middle section is more regular and the connection between this and the outer section is better (Figure 4.20 – 1). The connection in Figure 4.20 – 2 is adequate when compared with previous depositions but could stand to be improved. Despite the improvements there was a considerable difference in height between the middle and the outer sections (see Figure 4.22).

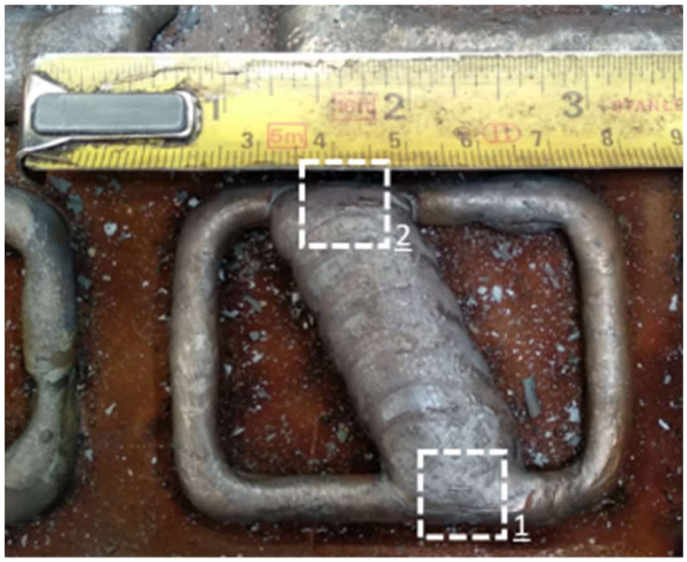

Figure 4.20 Fifth experiment of part deposition with PowerMill Additive

Figure 4.21 Shows the result of the sixth experiment. In this deposition the TS was kept at 0.0044 m/s like on the fifth deposition, but the stepover was increased to 5 mm in order to decrease to amount of material deposited in the area, in an attempt to reduce the height difference between sections. Figure 4.22 shows that, although a reduction in height difference was achieved, it came at the cost of an irregular middle section and a worse connection between them.

Figure 4.21 Sixth experiment of part deposition with PowerMill Additive

Figure 4.22 Difference in height between experiments 5 and 6

From the seventh and eight experiments the original part size was recovered while employing the second deposition path. In order to fill the full width of the outer section two weld beads were necessary, which introduced another set of problems.

Figure 4.23 shows the results of the seventh experiment. The overlap between the two weld beads that form the outer section of the part (Figure 4.23 – 1) isn't really satisfactory, meaning that the stepover wasn't properly defined for the parameters and bead width. The corners (Figure 4.23 – 2) are irregular and require correction. The connection between the outer and middle sections of the part isn't good enough, especially on the bottom side (Figure 4.23 – 3), where a considerable gap can be observed between them.

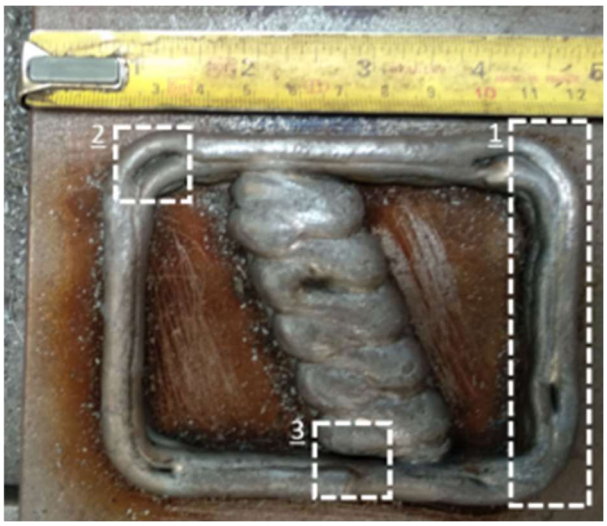

Figure 4.23 Seventh experiment of part deposition with PowerMill Additive

Figure 4.24 shows the result of the eight experiment. Despite an acceptable middle section (Figure 4.24 – 1) and somewhat better corners (Figure 4.24 – 2) than the seventh experiment, the overlap between the weld beads that form the outer section is still subpar (Figure 4.24 – 3). Despite the regular middle section, the connection to the outer section (Figure 4.24 – 4) still has an appreciable gap between them.

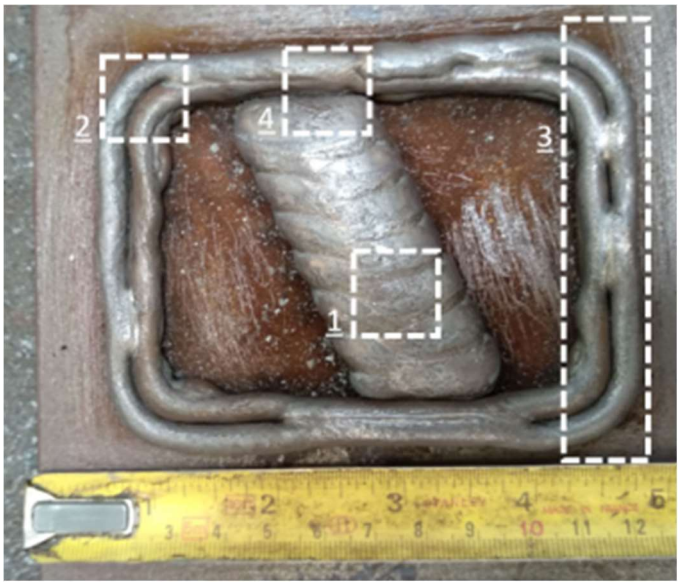

Figure 4.24 Eight experiment of part deposition with PowerMill Additive

4.3.2. Depositions made with WAAMPlanner

As mentioned in section 3.7, Cranfield's University WAAM Software, WAAMPlanner is limited to an oscillation strategy. Three experiments were performed, with the resulting depositions presented in Figure 4.25.

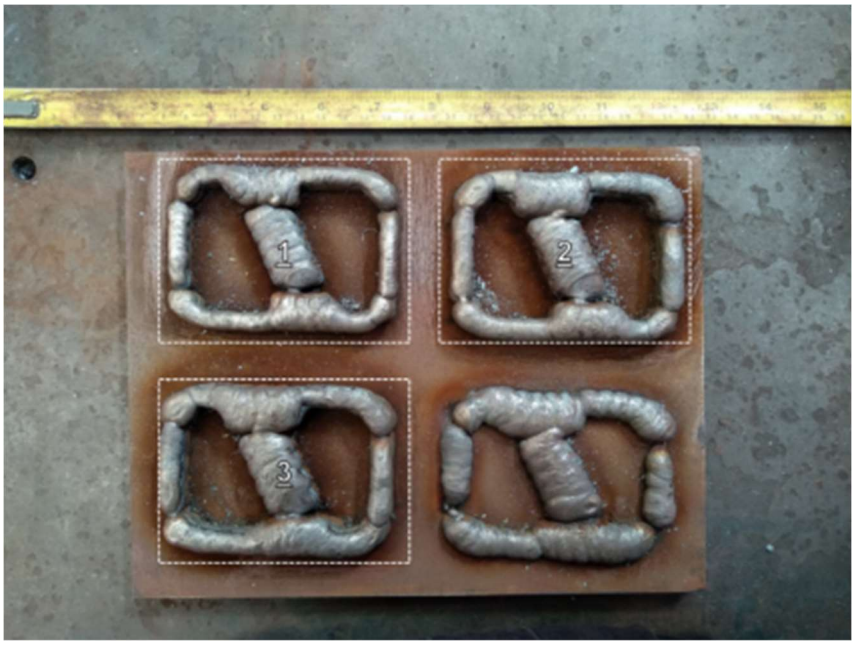

Figure 4.25 Experiments performed for part deposition with WAAMPlanner

The parameters used in this second stage of part deposition are presented in Table 4.8.

Table 4.8 Process parameters for the experiments with WAAMPlanner

Experiments	**Parameters**				
	CTWD [mm]	**SGFR [L/min]**	**WFS [m/min]**	**WFS/TS**	**TS [m/min]**
1	15	18	3	10	0.30
2			4	10	0.40
3				15	0.27

Three experiments were performed with the parameters that produced samples classified as acceptable in the visual inspection and that provided the best balance between percentage of deviation from the average measured values, like mentioned in section 4.1.2. The employed deposition strategy is depicted in Figure 3.10.

Observing the experiments, it becomes immediately apparent that there is a lack of connection between segments, a defect shared between all the depositions performed in this stage. This issue is later addressed in section 4.3.3.

Figure 4.26 shows the results of the first experiment.

Figure 4.26 First experiment of part deposition with WAAMPlanner

Like mentioned previously, lack of connection between segments is the main issue to be addressed, near the corners, where the connection is minimal (Figure 4.26 – 1), and in the center (Figure 4.26 – 2) where the connection between the outer and middle section is minimal to non-existent, with the substrate visible underneath it in some areas. Due to the characteristics of the robotic system, its linear velocity is reduced when it performs a curvilinear motion and when the arc is ignited in the starting position of the weld path. Starting close to the corners combines these two factors which leads to an excessive buildup of material near that region (Figure 4.26 – 3). Despite these defects, the linear segments and middle section of the part do not present irregularities and the height is also kept uniform throughout the successive layers, without excessive buildup of material in the Z direction.

Figure 4.27 shows the result of the second experiment.

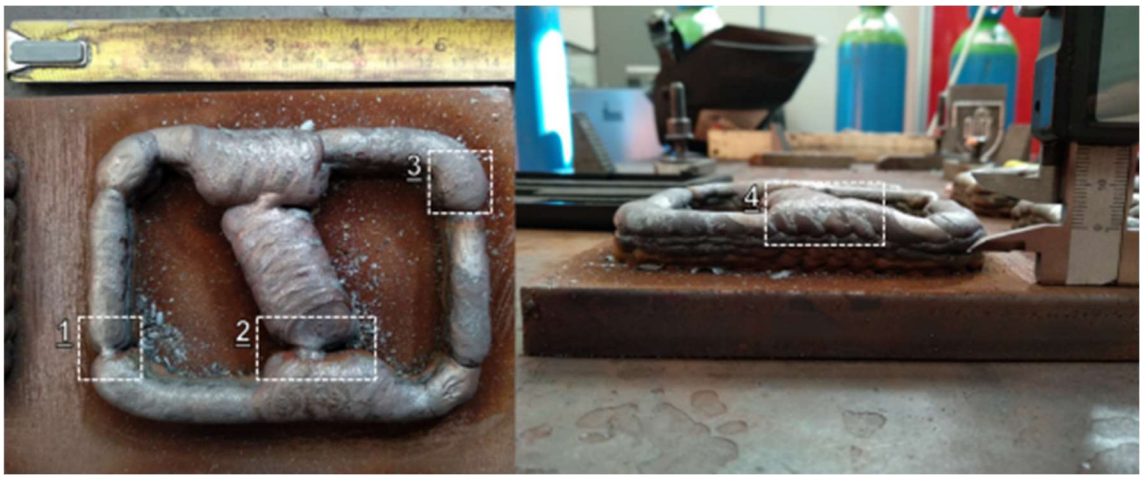

Figure 4.27 Second experiment of part deposition with WAAMPlanner

A higher WFS led to more material being deposited per unit of area, which in turn led to very slight improvements in the connection between segments, although, still far from being fully connected (Figure 4.27 – 1, Figure 4.27 – 2). For the same reason, an increase in the material buildup near the corners

(Figure 4.27 – 3) also occurred, as well as an excessive buildup of material in the Z direction (Figure 4.27 – 4), with an appreciable difference in height between the outer section of the part and the area where it intersects with the middle section. Like the previous experiment, the linear segments of the part are regular and do not present any visible defects beyond those already stated.

Figure 4.28 shows the result of the third experiment.

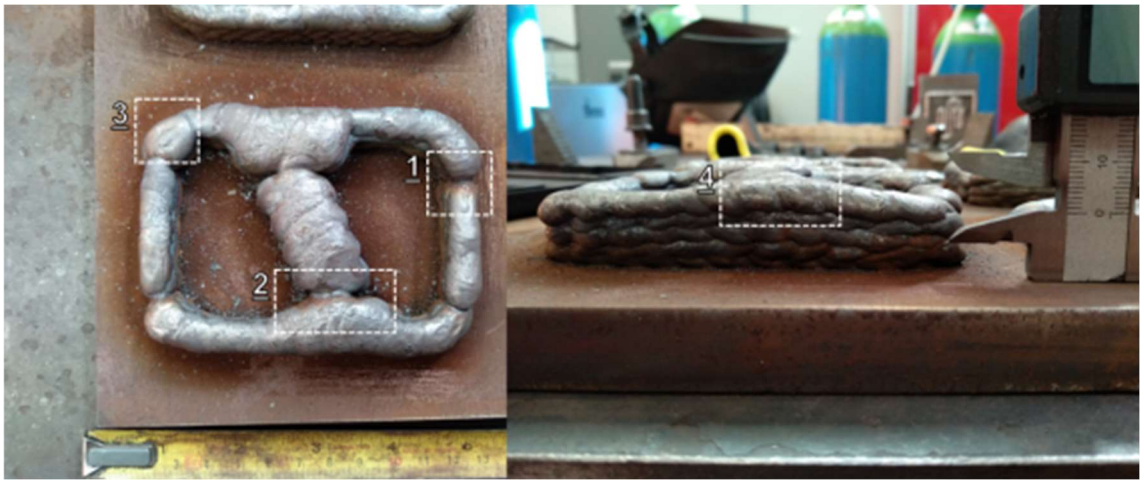

Figure 4.28 Third experiment of part deposition with WAAMPlanner

Maintaining the WFS from the previous experiment, while lowering the TS of the torch, only led to an aggravation of the issues already present, without any evident benefit. Lack of connection between segments (Figure 4.28 – 1, Figure 4.28 – 2), excessive material buildup near the corners (Figure 4.28 – 3) and in the Z direction where the middle section intersects the outer section Figure 4.28 – 4) are all still present and, unlike the transition from the first to the second experiment, where a slight improvement in segment connection was visible, that behavior is not observable here. Although the linear segments of the part do not show any irregularities, following the trend observed in previous experiments, they also do not show any improvement.

These experiments were measured in order to determine average width, height, length and percentage deviation. Three measurements were taken along the width and length and eleven measurements for height were taken in different points of the part as shown in Figure 4.29. These measurements, their averages and percentages of deviation are presented in Table 4.9. Percentage of deviation is represented graphically in Figure 4.30.

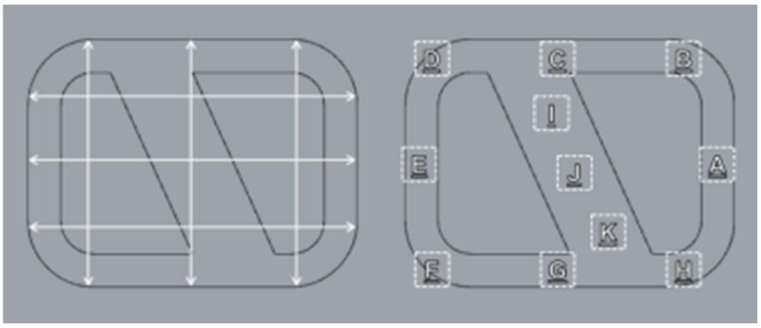

Figure 4.29 Measurements of the part

Table 4.9 Dimensions for the width, height and length for the depositions made with WAAMPlanner

Dimension	Experiments			
	1	2	3	
Width [mm]	70,88	72,30	71,43	
	71,09	71,75	71,80	
	70,89	72,49	71,67	
Average Width [mm]	70,95	72,18	71,63	
% of Deviation	9%	29%	14%	
Height [mm]	14,94	14,49	15,38	A
	14,21	14,00	16,13	B
	14,82	17,12	18,90	C
	14,45	14,13	15,83	D
	14,88	14,28	14,72	E
	14,30	14,76	15,76	F
	15,29	17,28	18,54	G
	14,99	15,34	15,96	H
	13,59	16,16	17,65	I
	14,13	16,65	18,36	J
	14,39	15,40	16,84	K
Average Height [mm]	14,54	15,42	16,73	
% of Deviation	40%	101%	120%	
Length [mm]	97,51	99,28	100,61	
	97,93	99,96	99,68	
	97,66	97,26	99,79	
Average Length [mm]	97,70	98,83	100,03	
% of Deviation	15%	105%	39%	

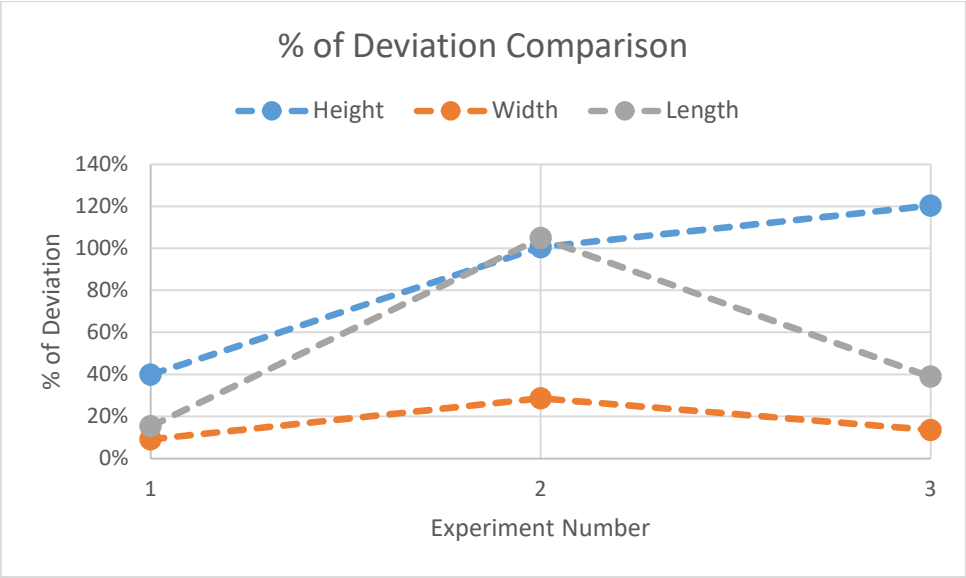

Figure 4.30 Percentage of Deviation Comparison between experiments

From Table 4.9 and Figure 4.30 it can be seen that experiment 1 presents the lowest values for percentage of deviation for every measurement, making its parameters prime candidates for the final part deposition. It can also be observed that percentage of deviation for height assumes a high value in every experiment. Figure 4.31 shows the values of measured height in the positions identified in Figure 4.29.

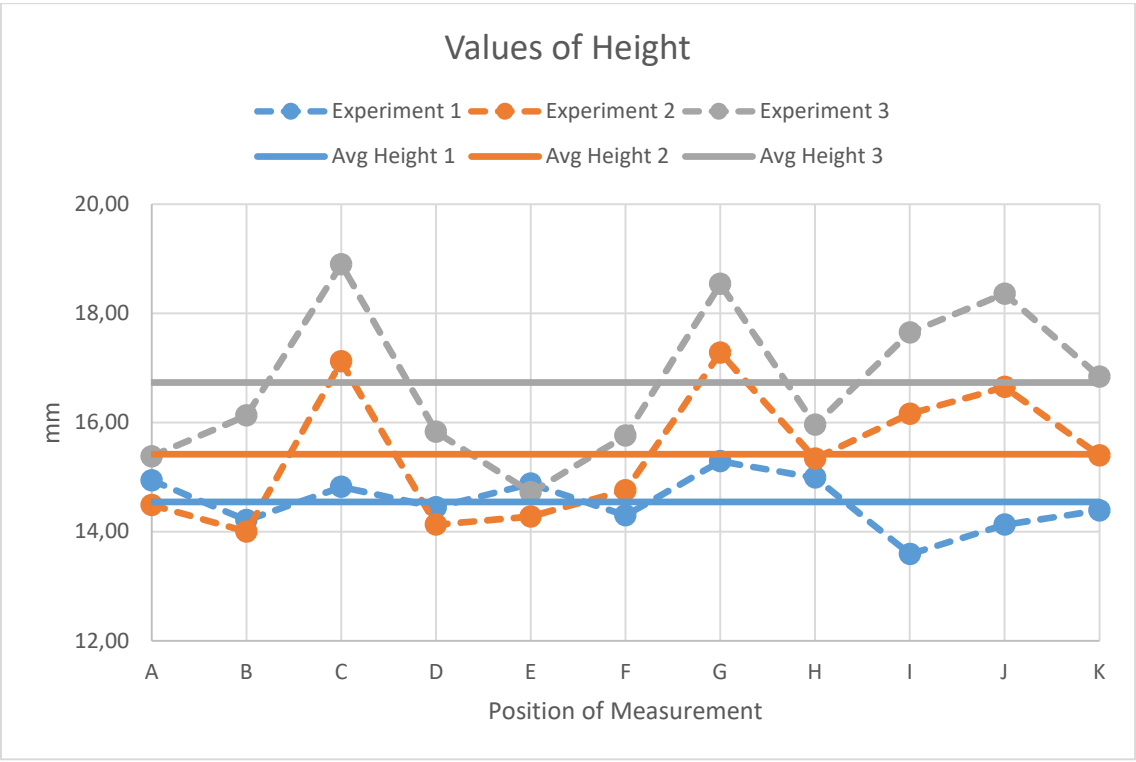

Figure 4.31 Values of measured height

From Figure 4.31 we can observe that positions C, G, I, J and K are the ones that deviate the most from the average values. These positions correspond to the areas where the middle section intersects the outer section (C and G) and the middle section itself (I, J and K), identifying them as problem areas, where material buildup in the Z direction is most pronounced, and will require special attention when creating the final part.

4.3.3. Final Part Deposition

For the deposition of the final part two issues required attention, the lack of connectivity between segments and the buildup of material in the corners of the part. Being the most glaring defect, lack of connectivity was tackled first and excessive material buildup second.

Due to its finer degree of control over the deposition path WAAMPlanner was selected for final part deposition.

Seven experiments were performed with their results being presented in Figure 4.32, Figure 4.33 and Figure 4.34.

Figure 4.32 Experiments 1-3 of final part deposition

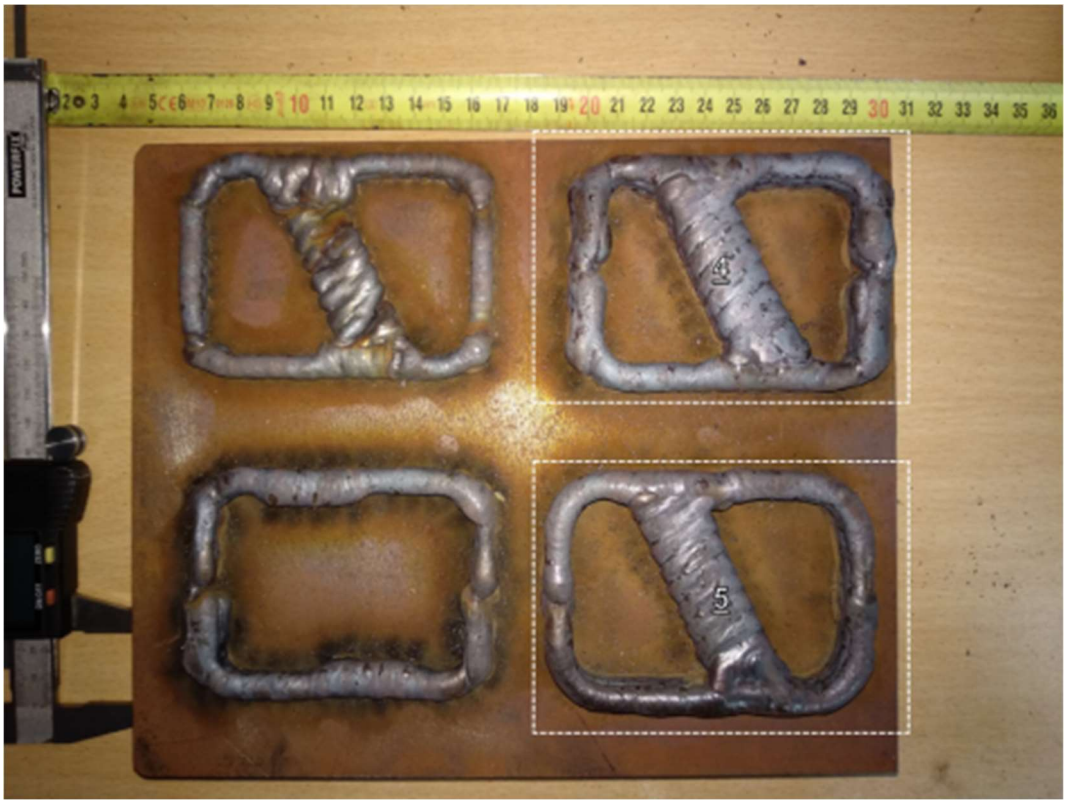

Figure 4.33 Experiments 4-5 of final part deposition

Figure 4.34 Experiments 6-7 of final part deposition

In order to improve segment connectivity two approaches were tested, increasing overlap between the segments by adjusting the deposition path and lowering the TS of the torch in these areas in order to provide more material per unit of area and close the gaps. The parameters used in these experiments are presented in Table 4.10.

Table 4.10 Process parameters for the final part deposition experiments

Experiments	Parameters			
	CTWD [mm]	SGFR [L/min]	WFS [m/min]	TS [m/min]
1	15	18	3.00	0.30
2			3.00	0.30
3			3.00	0.40
4			3.50	0.40
5			3.50	0.40
6			3.00	0.40
7			3.50	0.40

Figure 4.35 shows the result of experiment 1. For this test the WFS and TS were the ones that provided the most regular depositions during the testing made with WAAMPlanner, as mentioned in section 4.3.2, as was the employed strategy (see Figure 3.10). The segmentation layers were manipulated to increase the overlap between segments in order to close the gaps that were visible.

Figure 4.35 First experiment for final part deposition

No visible gaps can be observed on this first experiment, both on the connection between the middle and outer section (Figure 4.35 – 1), and on the corners of the part (Figure 4.35 – 2). No excessive

buildup of material on the critical areas identified in section 4.3.2 (C, G, I, J, K, see Figure 4.29) can be observed, although, since no measures were taken to reduce excessive material buildup in the corners, on this experiment, increasing the overlap led to an aggravation of this defect (Figure 4.35 – 3).

Figure 4.36 shows the result of experiment 2. The WFS and TS of the previous experiment were maintained, except in the segment intersection zones, where, making use of the CustomZone feature of WAAMPlanner described in section 3.7, the TS was defined to be 0.15 m/min, which is half of the one used in the remainder of the part.

Figure 4.36 Second experiment for final part deposition

It is immediately visible that this solution introduces more problems than solutions. A large excess of material is present, not only in the corners as it was before (Figure 4.36 – 2), but also in the connection between the middle and outer section (Figure 4.36 – 1, Figure 4.36 - 4). Although no visible gaps are observed between segments (Figure 4.36 – 3), the connection doesn't seem particularly improved over the previous experiment, which leads us to conclude that, although theoretically possible to join segments together through the use of a lower TS of the torch in connection areas, optimizing the deposition path to avoid this defect, while maintaining the same TS throughout the part, seems like a more viable strategy, making it the main focus of the remainder experiments to solve this problem.

In order to reduce excess material buildup in the corners of the part, it was first attempted to use the strategy of the first experiment with the increased overlap between segments, while increasing the TS of the torch to 0.40 m/min to compensate the slowing down of the robotic system linear velocity when performing a curvilinear movement, depositing less material per unit of area as a consequence. The results of this experiment are present in Figure 4.37.

Figure 4.37 Third experiment for final part deposition

When compared to the first experiment, the improvements on the excessive material buildup (Figure 4.37 – 1) are marginal to non-existent. The connection between segments (Figure 4.37 – 2, Figure 4.37 – 3) also seems unaffected.

Since no obvious improvements were visible with the increased TS of the torch, it was attempted to develop new strategies of deposition. The first of these strategies, depicted in Figure 4.38, ensures that the starting and finishing points of the weld path are near the center of linear portions of the outer section and not on the corners, so that the effects of the lower speed of the robot, when the arc is ignited and when it performs curvilinear motions, are not combined in an attempt to reduce excess material buildup. This strategy also reduces the number of segments from five to three, minimizing the number of starts and stops of the torch. The WFS was increased to 3.5 m/min since the middle section was showing lack of material, negatively affecting its geometry. The layer height defined in the software was also increased to 3 mm, after measuring and concluding that 2 mm were not enough to keep CTWD constant.

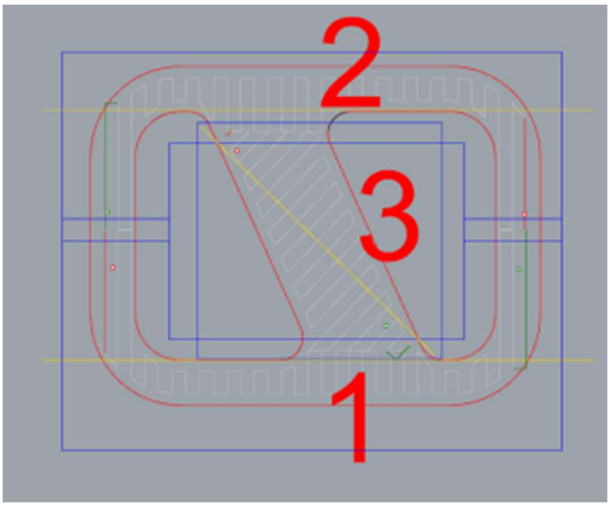

Figure 4.38 Alternative strategy for final part deposition

The result of the experiment performed with this new strategy is present in Figure 4.39.

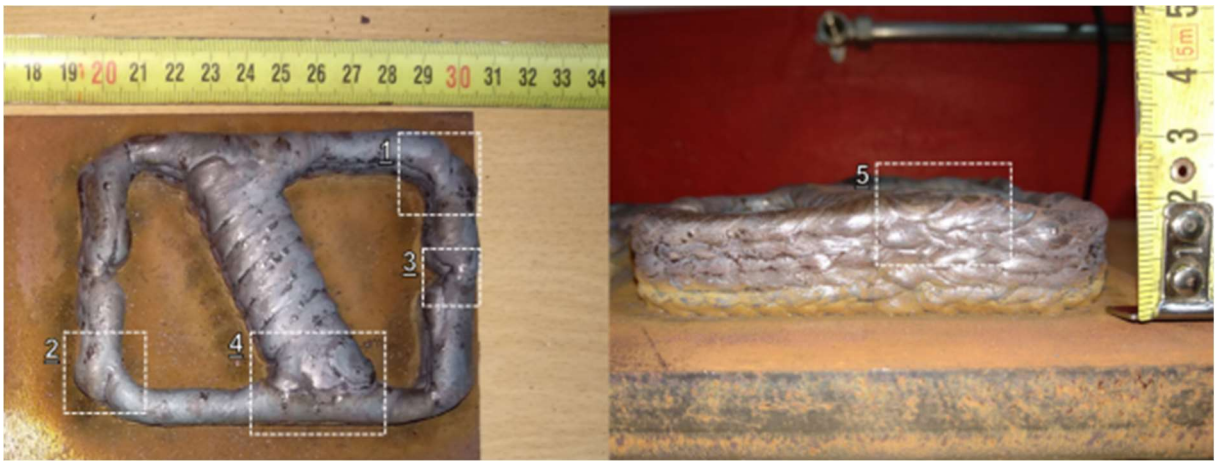

Figure 4.39 Fourth experiment for final part deposition

Although some improvements related to excess material buildup near the corners can be observed in some areas (Figure 4.39 – 1), others still present a somewhat irregular geometry (Figure 4.39 – 2). A possible explanation is that, both on the left and right side, the oscillation path is parallel to the long edge of the part, which is not a good practice to follow. The deficient connection between segments on the sides (Figure 4.39 – 3) can also be explained by this factor. The connection between the middle and outer section (Figure 4.39 – 4), as well as the geometry of the middle section itself, is improved due to the increase of the WFS, though this also led to an excess material buildup in this area (Figure 4.39 - 5).

In order to address the issues introduced by the previous strategy, a new one was developed, and it is presented in Figure 4.40.

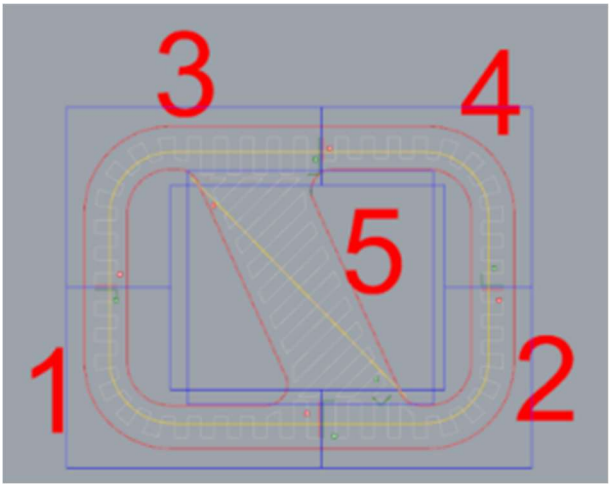

Figure 4.40 Second alternative strategy for final part deposition

With this strategy the outer section of the part is deposited following an oscillation path perpendicular to the longest edge of the part all around. However, due to limitations of the software, the number of segments had to be increased to five once more. The middle section remained unchanged from the previous strategy. The result of this experiment is presented in Figure 4.41.

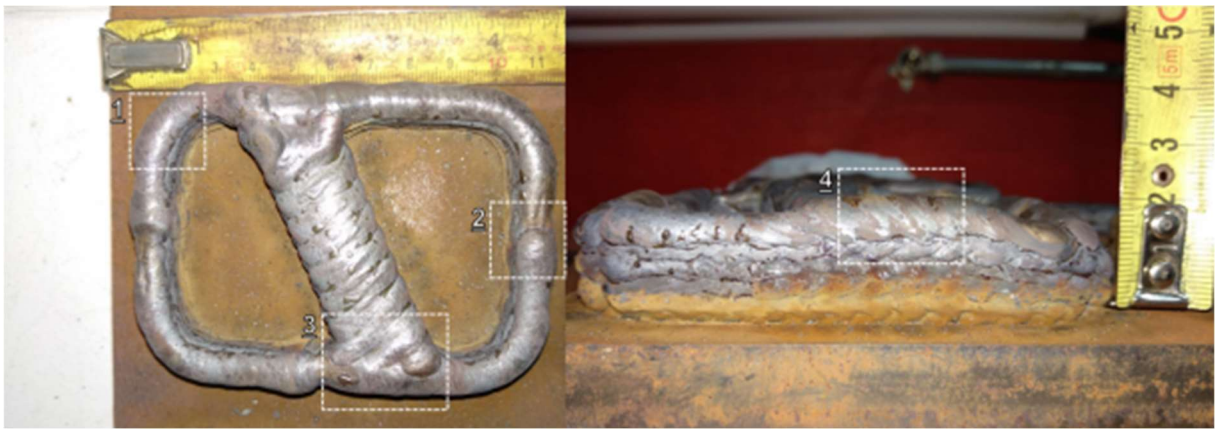

Figure 4.41 Fifth experiment of final part deposition

A number of improvements over the previous experiments can be observed. The excess material buildup near the corners has been eliminated (Figure 4.41 – 1), the connection between segments at the sides is also improved over the fourth experiment, with no visible gap between them (Figure 4.41 – 2) and the good connection between the middle and outer section is maintained from the previous experiment (Figure 4.41 – 3). Despite these improvements, excess material buildup in the Z direction is still present (Figure 4.41 – 4).

With the connections between segments and excess material buildup in the corners fixed, only the buildup in the Z direction issue remained to be addressed. In an attempt to solve this problem a modification of the previous strategy was introduced, presented in Figure 4.42.

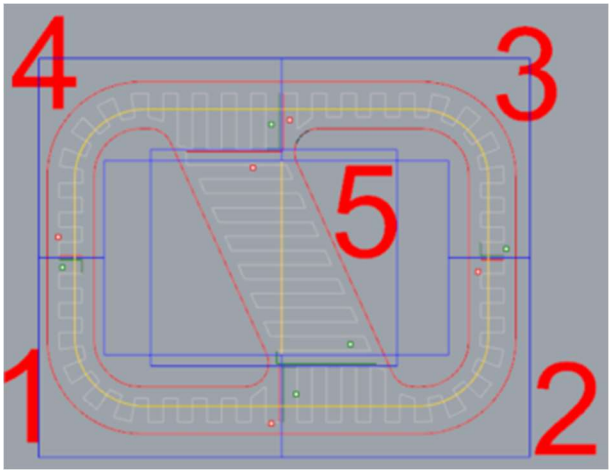

Figure 4.42 Third alternative for final part deposition

This strategy modified the extremes of the deposition path of the middle section, making them follow a linear path close to the outer section, as opposed to the weaving path of previous strategies, in an attempt to reduce the amount of material deposited in this area, while maintaining a connection between the sections. For the first experiment with this new strategy, the parameters were brought back to the initial ones of 3 m/min and 0.005 m/s for WFS and TS, respectively. The results are presented in Figure 4.43.

Figure 4.43 Sixth experiment for final part deposition

This experiment yielded mixed results. Although the corners show a very regular geometry (Figure 4.43 – 1), the connection between segments doesn't evidence any gaps (Figure 4.43 – 2) and the excess material buildup in the Z direction is reduced when compared to previous depositions (Figure 4.43 – 3), the connection between the middle and outer sections has deteriorated considerably (Figure 4.43 – 4). The geometry of the middle section has also degraded, with lack of material being the cause.

In the seventh experiment the WFS and TS were brought back to 3.5 m/min and 0.0067 m/s, respectively, in order to address these defects. The results are presented in Figure 4.44.

Figure 4.44 Seventh experiment for final part deposition

This experiment shows the same characteristics of the previous one, regular corners (Figure 4.44 – 1), complete connection between segments of the outer section (Figure 4.44 – 2) and reduced excess material buildup in the Z direction (Figure 4.44 – 3). Although improvements were made regarding the middle section geometry and the connection between it and the outer section (Figure 4.44 – 4), there are still some areas where gaps are visible.

These depositions were measured with the same methodology as the ones in section 4.3.2, with three measurements taken along the width and length, and eleven measurements for height at specific points of the part (see Figure 4.29) to calculate average dimensions and percentages of deviation. These measurements are presented in Table 4.11 and percentage of deviation for each experiment are represented graphically in Figure 4.45.

Table 4.11 Dimensions for the width, height and length for the depositions made for final part deposition

Dimension	Experiments							
	1	2	3	4	5	6	7	
Width [mm]	69,64	71,31	70,20	72,13	71,53	96,56	72,68	
	69,97	70,80	69,73	70,93	71,32	99,13	72,63	
	70,43	70,32	70,34	71,47	70,64	97,16	72,86	
Average Width [mm]	70,01	70,81	70,09	71,51	71,16	97,62	72,72	
% of Deviation	28%	33%	24%	41%	35%	101%	9%	
Height [mm]	16,07	14,79	15,50	19,24	19,55	18,06	14,43	A
	15,64	15,55	16,01	18,50	19,04	17,62	14,03	B
	15,78	15,04	14,84	21,21	20,82	19,38	15,03	C
	15,56	14,63	15,87	17,70	19,48	17,80	14,24	D
	15,88	14,77	16,07	18,88	19,83	18,37	13,97	E
	15,79	13,87	15,40	18,72	18,80	17,67	13,56	F
	15,65	15,00	15,48	20,73	20,99	18,27	14,89	G
	15,27	13,72	15,42	17,53	19,21	16,90	13,15	H
	16,03	20,12	14,72	18,68	19,45	15,46	14,66	I
	14,12	14,00	14,27	19,14	19,81	16,28	14,68	J
	14,74	17,62	14,98	20,15	21,17	17,36	16,78	K
Average Height [mm]	15,50	15,37	15,32	19,13	19,83	17,56	14,49	
% of Deviation	43%	130%	45%	87%	63%	77%	65%	
Length [mm]	97,63	101,29	97,76	97,21	97,93	96,55	98,78	
	97,30	98,41	97,17	97,81	99,96	99,12	101,53	
	98,32	101,54	97,18	98,14	98,08	96,96	98,84	
Average Length [mm]	97,75	100,41	97,37	97,72	98,66	97,54	99,72	
% of Deviation	38%	134%	26%	34%	87%	105%	121%	

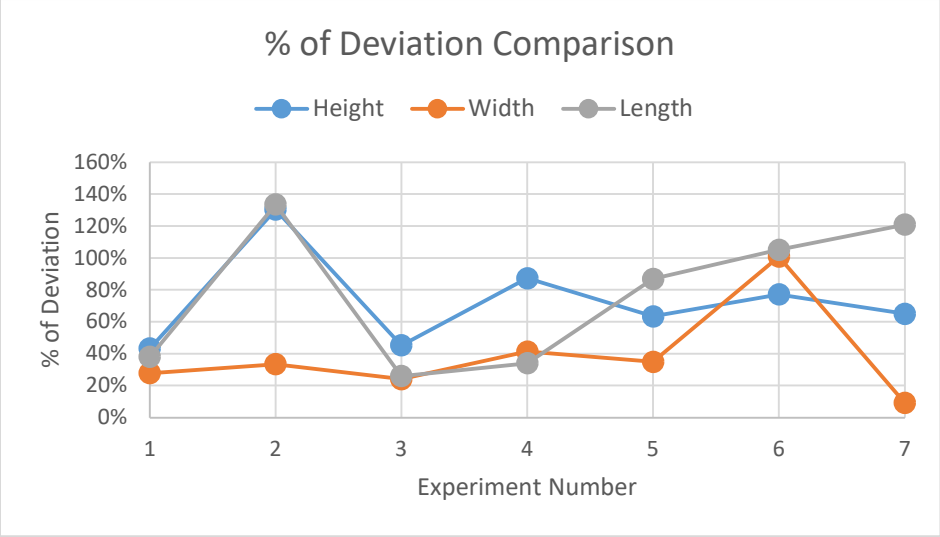

Figure 4.45 Percentage of Deviation Comparison between experiments

From Figure 4.45 and Table 4.11 it can be observed that, with the exception of experiment number six, the width was the dimension that deviated the least, assuming low values of percentage deviation across all the other experiments. The length was the dimension that varied the most, especially in experiment number two, where custom zones were defined in an attempt to close the gaps between the segments and excess material buildup was introduced as a consequence, skewing the values, not only for length but also for height. Discarding experiment two, the percentage deviation for height saw an increase starting from experiment five, which coincided with the increase in WFS to 3.5 m/min and the excess material buildup in the Z direction that happened as a consequence.

Taking into account the observations made while analyzing each experiment and the data obtained from the measurements, the parameters and strategy from experiment number five were selected for the deposition of the final part. The main issue related to this experiment was the excess material buildup in the Z direction, which can be solved by removing the top layers of the part after deposition.

The parameters used for the deposition of the final part are presented in Table 4.12.

Table 4.12 Final part parameters

Parameters	Values
CTWD [mm]	15
SGFR [L/min]	18
WFS [m/min]	3,5
TS [m/min]	0,40
Layer Height [mm]	3

During deposition was observed that the characteristics of experiment five, that served as base for this deposition, are mostly maintained with the increase in height. It was observed that the corners and linear segments of the part retain their regularity, the connection between segments is complete, without visible gaps between them. Nevertheless, the increase in height caused the accumulation of the excess material buildup in the Z direction that was present before. Another defect introduced indirectly by the increase in height is presented in Figure 4.46 – 1.

Figure 4.46 Defect on final part

In Figure 4.46 it's visible that the middle section has collapsed. Like stated before this defect was introduced indirectly by the increase in height, since the additional thermal cycles created by it led to lower thermal gradients and, consequently, higher heat accumulation. This heat accumulation increased the solidification time of the metal, which led to its collapse. The reason why this defect is not present in other areas of the part is that a higher amount of material is deposited in this section. To solve this defect, the waiting time between layers was increased, to allow for more cooling. In order to control the temperature between each successive layer deposition a Hanna HI 935005 thermocouple thermometer was used. The interlayer temperature was kept at around 200 ºC. The parameters and deposition path remained the same as the previous attempt. The resulting deposition is presented in Figure 4.47 and Figure 4.48.

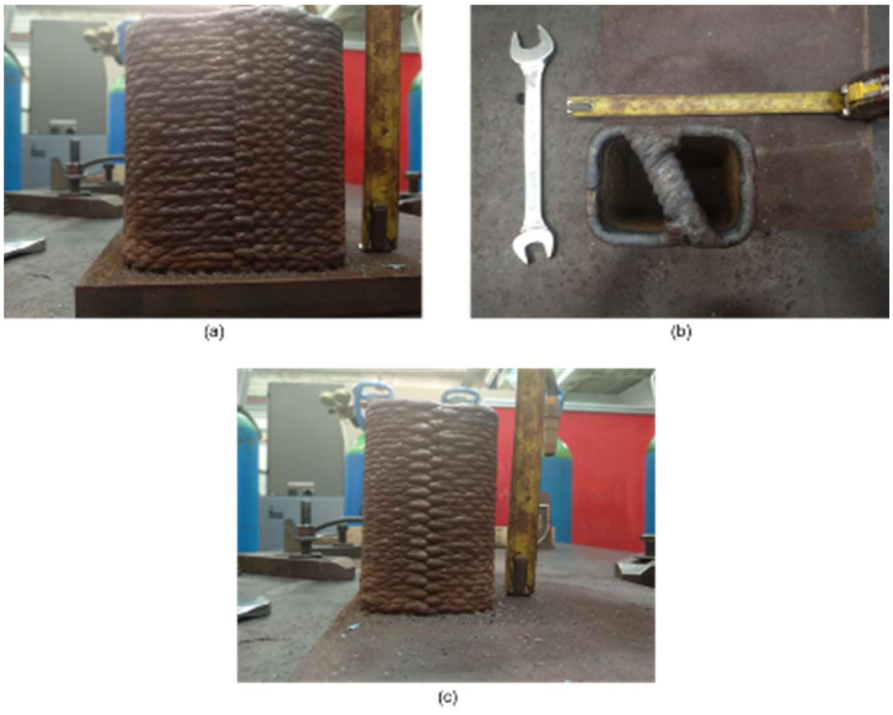

Figure 4.47 Final part (a) – front view, (b) – top view, (c) – side view

Figure 4.48 Area of the previously observed defect

Observing Figure 4.47 it can be seen that the geometric characteristics of the previous attempt are still present even with the further increase in height. During deposition it was observed that excess of material buildup in Z could be fixed by introducing “corrective segments” every two consecutive layers, meaning different segments from the regular ones which would level the top layer of the part. It would be advantageous if the software could take this into account, perhaps by allowing the creation of a “sublayer” after a consecutive number of user defined layers where these corrective segments could be introduced, similarly to the strategy outlined in section 2.3.2.5 for the manufacturing of 90º walls.

Figure 4.48 shows that controlling the interlayer temperature corrected the defect that was present in the previous attempt of final part deposition, without any visible material collapse. This temperature control was also employed between segments, since the deposition of material also heats up the zone adjacent to it. This intersegment temperature control was especially relevant when depositing the middle section of the part.

Although the proposed geometry was successfully deposited, a reduction on the dimensions of the part was observed. This reduction was especially noticeable in the width of the part due to the contraction of the middle section after cooling, which exerted a force in the outer section of the part where they were connected.

4.3.4. Part Deposition Summary

Although both programs managed to generate a path capable of producing a complete version of the part, the superior control over part segmentation and path deposition gave Cranfield’s University software, WAAMPlanner, the advantage over Autodesk’s PowerMill. WAAMPlanner, having a more manual approach to segmentation allows the user to precisely control how a part should be segmented, which is convenient when depositing geometries with a higher degree of complexity. Despite not being a feature used extensively in this work, the possibility of defining zones with custom parameters is also a useful tool for a WAAM software to have. Although some degree of control is provided, PowerMill lacks certain features that a fully-fledged AM software should possess. For example, PowerMill is unable to change partitions of the part to better suit the user needs and to define zones with custom parameters,

which leads to difficulties when depositing more complex parts, where intersections, T-junctions and corners may require special attention and tight parameter control in order to achieve adequate deposition. Nevertheless, PowerMill's more automatic approach to defining deposition paths can be useful when depositing simpler parts or when the user has little experience with WAAM.

Although both software's are already usable, some features still need to be implemented in order to consider them complete. A database of parameters for WAAM commonly used materials would allow the end user to focus on deposition path immediately, instead of parametrization, although this would require extensive research in order to implement it for every material. More deposition strategies beyond oscillation, like weaving, the researched strategies and decomposition methods of CAD models presented in section 2.3.2.5 and the introduction of corrective segments could also be implemented to allow for more options during deposition.

The most challenging aspects of depositing a part such as the one presented in this work are intersections, connection between segments, excess of material buildup in certain critical areas, such as corners and material collapsing. In order to overcome these challenges, the following methodology was employed:

1. Reduce the number of segments to the bare minimum in order to diminish the number of starts and stops of the torch;
2. Defining the overlap of the segments in a way that guarantees the absence of gaps between them. This step may require some trial and error from the user's part;
3. Starting the deposition paths away from corners, intersections and other critical areas. Attempt to start in a low complexity area;
4. Control the temperature between layers, giving the part enough time to cool down before depositing the next layer.

5. Conclusion and Future Work

5.1. Conclusions

This work envisaged the production of a part made with AISI 410 stainless steel through WAAM, which was successfully achieved. The manufacturing of this part was accomplished through an initial stage of parametrization work and a second stage of deposition strategy fine tuning. Material characterization of the deposited material was also carried out. The following conclusions can be taken from this study:

1. The main factor that influences the geometry of linear weld beads is the TS of the torch, playing a pivotal role in both height and width of depositions, in a greater extent than WFS;
2. Parameters that produce sound linear walls do not necessarily produce acceptable walls produced using an oscillation deposition path, requiring a thoughtful selection of the stepover value to achieve a flat top surface with sufficient overlap;
3. Microstructure and macrostructure were in alignment with the literature, with no microstructural defects, such as cracks or lack of fusion, present in the analyzed samples;
4. Hardness values (372 HV to 412 HV) were in agreement with the ones found in literature [52], and characteristic of a martensitic structure, which grants parts created with this material high resistance to wear. The hardness values were also found to be independent of the employed process parameters;
5. Tensile testing revealed high values for both UTS and YS in both directions. It also showed mild ductility in a transversal direction (Z-direction) and significant ductility in the longitudinal direction (X-direction), although the former is more relevant to the study since parts are built in the Z direction;
6. Comparing both software's, WAAMPlanner appears to be the top choice as of now. Offering more control over segmentation of the part and process parameters, WAAMPlanner software showed better performance at part depositing than Autodesk's PowerMill Additive, although, being tested in an earlier stage of this work, may have contributed to this result. Nevertheless, PowerMill Additive more automated approach should not be discarded, since it could prove useful when depositing simpler parts;
7. WAAM software still has issues that need addressing. More strategies, especially weaving, could be available beyond oscillation and more freedom in path planning is required. A material database could also be beneficial in order to simplify the deposition process;
8. Although process parameters have a considerable influence in part quality, an appropriate deposition strategy must be defined in order to achieve successful deposition;
9. Heat accumulation also plays a role during deposition, and temperature between layers should be controlled in order to avoid defects.

As for deposition strategies the following aspects should be taken into account:

1. As stated before, a combination of process parameters and deposition path must be achieved in order to successfully produce a part;
2. Minimizing the number of start and stops of the torch is also advisable, in order to reduce the number of segments and connection points;
3. Deposition paths should take into account the limitations of the motion system. The KUKA robot used in this work showed a reduction in its linear velocity when striking the arc and when performing curvilinear motions, so these factors must be addressed to ensure successful depositions. For example, starting too close to a corner would lead to these two effects combining and excess material to accumulate there.

5.2. Future Work

1. Despite its recent advancements, WAAM still requires further research in order to be fully employed in an industrial setting. A few suggestions for future work are as follows: Perform further material characterization tests, such as Charpy impact tests and wear tests;
2. Develop a system to control temperatures and thermal cycles during deposition;
3. Using an efficient heat dissipation method, reducing cooling time between layers and cutting down part manufacturing time;
4. Conduct further research in intersections and how to optimize their deposition;
5. Further improve the WAAM software.
6. Building a part with more complex geometries, such as overhang structures;

6. Bibliography

[1] M. Attaran, “The rise of 3-D printing: The advantages of additive manufacturing over traditional manufacturing,” *Bus. Horiz.*, vol. 60, no. 5, pp. 677–688, 2017.

[2] D. Ding, Z. Pan, D. Cuiuri, and H. Li, “Wire-feed additive manufacturing of metal components: technologies, developments and future interests,” *Int. J. Adv. Manuf. Technol.*, vol. 81, no. 1–4, pp. 465–481, 2015.

[3] S. W. Williams, A. C. Addison, F. Martina, G. Pardal, J. Ding, and P. Colegrove, “Wire + Arc Additive Manufacturing,” *Mater. Sci. Technol.*, vol. 32, no. 7, pp. 641–647, 2015.

[4] ASTM INTERNATIONAL, “ASTM F2792-12a,” *Rapid Manuf. Assoc.*, vol. 9, pp. 1–3, 2013.

[5] T. Wohlers and T. Gornet, “History of Additive Manufacturing 2014,” *Wohlers Rep. 2014 - 3D Print. Addit. Manuf. State Ind.*, pp. 1–34, 2014.

[6] K. V. Wong and A. Hernandez, “A Review of Additive Manufacturing,” *ISRN Mech. Eng.*, vol. 2012, pp. 1–10, 2012.

[7] D. Bourell *et al.*, “Materials for additive manufacturing,” *CIRP Ann. - Manuf. Technol.*, vol. 66, no. 2, pp. 659–681, 2017.

[8] S. Bose, D. Ke, H. Sahasrabudhe, and A. Bandyopadhyay, “Additive manufacturing of biomaterials,” *Prog. Mater. Sci.*, vol. 93, pp. 45–111, 2018.

[9] I. Gibson, D. Rosen, and B. Stucker, *Additive manufacturing technologies: 3D printing, rapid prototyping, and direct digital manufacturing, second edition*. 2015.

[10] W. Gao *et al.*, “The status, challenges, and future of additive manufacturing in engineering,” *CAD Comput. Aided Des.*, vol. 69, pp. 65–89, 2015.

[11] P. Huang, D. Deng, and Y. Chen, “Modeling and Fabrication of Heterogeneous Three-Dimensional Objects Based on Additive Manufacturing,” in *Volume 2A: Advanced Manufacturing*, 2013, p. V02AT02A056.

[12] W. Liu and J. N. DuPont, “Fabrication of functionally graded TiC/Ti composites by laser engineered net shaping,” *Scr. Mater.*, vol. 48, no. 9, pp. 1337–1342, 2003.

[13] E. Brandl, B. Baufeld, C. Leyens, and R. Gault, “Additive manufactured Ti-6A1-4V using welding wire: Comparison of laser and arc beam deposition and evaluation with respect to aerospace material specifications,” *Phys. Procedia*, vol. 5, no. PART 2, pp. 595–606, 2010.

[14] P. Edwards and M. Ramulu, “Fatigue performance evaluation of selective laser melted Ti-6Al-4V,” *Mater. Sci. Eng. A*, vol. 598, pp. 327–337, 2014.

[15] L. Thijs, F. Verhaeghe, T. Craeghs, J. Van Humbeeck, and J. P. Kruth, “A study of the

microstructural evolution during selective laser melting of Ti-6Al-4V," *Acta Mater.*, vol. 58, no. 9, pp. 3303–3312, 2010.

[16] J. Yu, M. Rombouts, G. Maes, and F. Motmans, "Material Properties of Ti6Al4 v Parts Produced by Laser Metal Deposition," *Phys. Procedia*, vol. 39, pp. 416–424, 2012.

[17] T. Niendorf, S. Leuders, A. Riemer, H. A. Richard, T. Tröster, and D. Schwarze, "Highly anisotropic steel processed by selective laser melting," *Metall. Mater. Trans. B Process Metall. Mater. Process. Sci.*, vol. 44, no. 4, pp. 794–796, 2013.

[18] I. Yadroitsev, M. Pavlov, P. Bertrand, and I. Smurov, "Mechanical properties of samples fabricated by selective laser melting," *14èmes Assises Eur. du Prototypage Fabr. Rapide*, vol. 625, no. February 2016, pp. 24–25, 2009.

[19] E. Yasa and J. P. Kruth, "Microstructural investigation of selective laser melting 316L stainless steel parts exposed to laser re-melting," *Procedia Eng.*, vol. 19, pp. 389–395, 2011.

[20] L. E. Murr *et al.*, "Microstructures and properties of 17-4 PH stainless steel fabricated by selective laser melting," *J. Mater. Res. Technol.*, vol. 1, no. 3, pp. 167–177, 2012.

[21] A. B. Spierings, M. Schoepf, R. Kiesel, and K. Wegener, "Optimization of SLM productivity by aligning 17-4PH material properties on part requirements," *Rapid Prototyp. J.*, vol. 20, no. 6, pp. 444–448, 2014.

[22] T. L. Starr, K. Rafi, B. Stucker, and C. M. Scherzer, "Controlling phase composition in selective laser melted stainless steels," *23rd Annu. Int. Solid Free. Fabr. Symp. - An Addit. Manuf. Conf. SFF 2012*, pp. 439–446, 2012.

[23] A. Yadollahi, N. Shamsaei, S. M. Thompson, A. Elwany, L. Bian, and M. Mahmoudi, "Fatigue behavior of selective laser melted 17-4 PH stainless steel," *Solid Free Fabr Proc*, vol. 111, no. 479, p. 721, 2015.

[24] G. Casalino, S. L. Campanelli, N. Contuzzi, and A. D. Ludovico, "Experimental investigation and statistical optimisation of the selective laser melting process of a maraging steel," *Opt. Laser Technol.*, vol. 65, pp. 151–158, 2015.

[25] K. Kempen, E. Yasa, L. Thijs, J. P. Kruth, and J. Van Humbeeck, "Microstructure and mechanical properties of selective laser melted 18Ni-300 steel," *Phys. Procedia*, vol. 12, no. PART 1, pp. 255–263, 2011.

[26] E. Brandl, U. Heckenberger, V. Holzinger, and D. Buchbinder, "Additive manufactured AlSi10Mg samples using Selective Laser Melting (SLM): Microstructure, high cycle fatigue, and fracture behavior," *Mater. Des.*, vol. 34, no. 2, pp. 159–169, Feb. 2012.

[27] D. Buchbinder, H. Schleifenbaum, S. Heidrich, W. Meiners, and J. Bültmann, "High Power Selective Laser Melting (HP SLM) of Aluminum Parts," *Phys. Procedia*, vol. 12, no. PART 1, pp. 271–278, 2011.

[28] K. Kempen, L. Thijs, J. Van Humbeeck, and J. P. Kruth, “Processing AlSi10Mg by selective laser melting: Parameter optimisation and material characterisation,” *Mater. Sci. Technol. (United Kingdom)*, 2015.

[29] I. Maskery *et al.*, “Quantification and characterisation of porosity in selectively laser melted Al-Si10-Mg using X-ray computed tomography,” *Mater. Charact.*, 2016.

[30] B. Vandenbroucke and J. P. Kruth, “Selective laser melting of biocompatible metals for rapid manufacturing of medical parts,” in *17th Solid Freeform Fabrication Symposium, SFF 2006*, 2006.

[31] X. Z. Xin, N. Xiang, J. Chen, D. Xu, and B. Wei, “Corrosion characteristics of a selective laser melted Co-Cr dental alloy under physiological conditions,” *J. Mater. Sci.*, 2012.

[32] K. N. Amato *et al.*, “Microstructures and mechanical behavior of Inconel 718 fabricated by selective laser melting,” *Acta Mater.*, 2012.

[33] R. R. Dehoff *et al.*, “Site specific control of crystallographic grain orientation through electron beam additive manufacturing,” *Mater. Sci. Technol. (United Kingdom)*, 2015.

[34] S. Li, Q. Wei, Y. Shi, C. K. Chua, Z. Zhu, and D. Zhang, “Microstructure Characteristics of Inconel 625 Superalloy Manufactured by Selective Laser Melting,” *J. Mater. Sci. Technol.*, 2015.

[35] L. L. Parimi, G. Ravi, D. Clark, and M. M. Attallah, “Microstructural and texture development in direct laser fabricated IN718,” *Mater. Charact.*, 2014.

[36] M. Filomeno and S. Williams, “Wire + arc additive manufacturing vs. traditional machining from solid: a cost comparison,” 2015.

[37] M. Zenou and L. Grainger, *3 - Additive manufacturing of metallic materials*. Elsevier Inc., 2018.

[38] Y. Zhang *et al.*, “Additive Manufacturing of Metallic Materials: A Review,” *J. Mater. Eng. Perform.*, vol. 27, no. 1, pp. 1–13, 2018.

[39] R. Baker, “Method of Making Decorative Articles,” 1920.

[40] C. C. P. C. Brochure *et al.*, “United States Patent (19) Acheson 54 AUTOMATIC WELDING APPARATUS FOR,” no. 19, 1990.

[41] P. M. Sequeira Almeida and S. Williams, “Innovative process model of Ti-6Al-4V additive layer manufacturing using cold metal transfer (CMT),” in *21st Annual International Solid Freeform Fabrication Symposium - An Additive Manufacturing Conference, SFF 2010*, 2010.

[42] T. A. Rodrigues, V. Duarte, R. M. Miranda, T. G. Santos, and J. P. Oliveira, “Current status and perspectives on wire and arc additive manufacturing (WAAM),” *Materials (Basel).*, vol. 12, no. 7, 2019.

[43] D. Ding, Z. Pan, D. Cuiuri, H. Li, S. Van Duin, and N. Larkin, “Bead modelling and implementation

of adaptive MAT path in wire and arc additive manufacturing," *Robot. Comput. Integr. Manuf.*, vol. 39, pp. 32–42, 2016.

[44] Fronius, "CMT – COLD METAL TRANSFER: THE COLD WELDING PROCESS FOR PREMIUM QUALITY." [Online]. Available: https://www.fronius.com/en/welding-technology/our-expertise/welding-processes/cmt. [Accessed: 02-Sep-2019].

[45] N. Rodriguez, L. Vázquez, I. Huarte, E. Arruti, I. Tabernero, and P. Alvarez, "Wire and arc additive manufacturing: a comparison between CMT and TopTIG processes applied to stainless steel," *Weld. World*, 2018.

[46] B. W. Shinn, D. F. Farson, and P. E. Denney, "Laser stabilisation of arc cathode spots in titanium welding," *Sci. Technol. Weld. Join.*, 2005.

[47] H. Geng, J. Li, J. Xiong, X. Lin, and F. Zhang, "Optimization of wire feed for GTAW based additive manufacturing," *J. Mater. Process. Technol.*, 2017.

[48] C. V. Haden, G. Zeng, F. M. Carter, C. Ruhl, B. A. Krick, and D. G. Harlow, "Wire and arc additive manufactured steel: Tensile and wear properties," *Addit. Manuf.*, 2017.

[49] O. Yilmaz and A. A. Ugla, "Microstructure characterization of SS308LSi components manufactured by GTAW-based additive manufacturing: shaped metal deposition using pulsed current arc," *Int. J. Adv. Manuf. Technol.*, 2017.

[50] A. Queguineur, G. Rückert, F. Cortial, and J. Y. Hascoët, "Evaluation of wire arc additive manufacturing for large-sized components in naval applications," *Weld. World*, 2018.

[51] J. Ge, J. Lin, Y. Chen, Y. Lei, and H. Fu, "Characterization of wire arc additive manufacturing 2Cr13 part: Process stability, microstructural evolution, and tensile properties," *J. Alloys Compd.*, 2018.

[52] M. M. Amrei, H. Monajati, D. Thibault, Y. Verreman, L. Germain, and P. Bocher, "Microstructure characterization and hardness distribution of 13Cr4Ni multipass weld metal," *Mater. Charact.*, vol. 111, pp. 128–136, 2016.

[53] T. Wang, Y. Zhang, Z. Wu, and C. Shi, "Microstructure and properties of die steel fabricated by WAAM using H13 wire," *Vacuum*, vol. 149, pp. 185–189, 2018.

[54] X. Xu, J. Ding, S. Ganguly, C. Diao, and S. Williams, "Oxide accumulation effects on wire + arc layer-by-layer additive manufacture process," *J. Mater. Process. Technol.*, vol. 252, no. July 2017, pp. 739–750, 2018.

[55] W. Yangfan, C. Xizhang, and S. Chuanchu, "Microstructure and mechanical properties of Inconel 625 fabricated by wire-arc additive manufacturing," *Surf. Coatings Technol.*, vol. 374, no. May, pp. 116–123, 2019.

[56] H. Attar, M. J. Bermingham, S. Ehtemam-Haghighi, A. Dehghan-Manshadi, D. Kent, and M. S.

Dargusch, “Evaluation of the mechanical and wear properties of titanium produced by three different additive manufacturing methods for biomedical application,” *Mater. Sci. Eng. A*, vol. 760, no. May, pp. 339–345, 2019.

[57] J. C. Lütjering, Gerd, Williams, *Titanium*, 2nd ed. Springer-Verlag Berlin Heidelberg, 2007.

[58] S. A. M. Tofail, E. P. Koumoulos, A. Bandyopadhyay, S. Bose, L. O’Donoghue, and C. Charitidis, “Additive manufacturing: scientific and technological challenges, market uptake and opportunities,” *Mater. Today*, vol. 21, no. 1, pp. 22–37, 2018.

[59] S. Williams, “Large scale metal wire + arc additive manufacturing of structural engineering parts,” *69th IIW Annu. Assem. Int. Conf.*, p. 25, 2016.

[60] J. Ding *et al.*, “Thermo-mechanical analysis of Wire and Arc Additive Layer Manufacturing process on large multi-layer parts,” *Comput. Mater. Sci.*, 2011.

[61] Y. M. Zhang, Y. Chen, P. Li, and A. T. Male, “Weld deposition-based rapid prototyping: A preliminary study,” *J. Mater. Process. Technol.*, vol. 135, no. 2-3 SPEC., pp. 347–357, 2003.

[62] Z. Hu, X. Qin, T. Shao, and H. Liu, “Understanding and overcoming of abnormity at start and end of the weld bead in additive manufacturing with GMAW,” *Int. J. Adv. Manuf. Technol.*, vol. 95, no. 5–8, pp. 2357–2368, 2018.

[63] S. Suryakumar, K. P. Karunakaran, A. Bernard, U. Chandrasekhar, N. Raghavender, and D. Sharma, “Weld bead modeling and process optimization in Hybrid Layered Manufacturing,” *CAD Comput. Aided Des.*, 2011.

[64] J. Xiong, G. Zhang, J. Hu, and L. Wu, “Bead geometry prediction for robotic GMAW-based rapid manufacturing through a neural network and a second-order regression analysis,” *J. Intell. Manuf.*, 2014.

[65] J. Xiong, G. Zhang, H. Gao, and L. Wu, “Modeling of bead section profile and overlapping beads with experimental validation for robotic GMAW-based rapid manufacturing,” *Robot. Comput. Integr. Manuf.*, 2013.

[66] D. Ding, Z. Pan, D. Cuiuri, and H. Li, “A multi-bead overlapping model for robotic wire and arc additive manufacturing (WAAM),” *Robot. Comput. Integr. Manuf.*, vol. 31, pp. 101–110, 2015.

[67] X. Xu, J. Ding, S. Ganguly, C. Diao, and S. Williams, “Preliminary Investigation of Building Strategies of Maraging Steel Bulk Material Using Wire + Arc Additive Manufacture,” *J. Mater. Eng. Perform.*, pp. 1–7, 2018.

[68] D. Ding, Z. Pan, D. Cuiuri, and H. Li, “A tool-path generation strategy for wire and arc additive manufacturing,” *Int. J. Adv. Manuf. Technol.*, vol. 73, no. 1–4, pp. 173–183, 2014.

[69] J. Kao and F. B. Prinz, “OPTIMAL MOTION PLANNING FOR DEPOSITIONIN LAYERED MANUFACTURING,” 1998.

[70] G. Venturini, F. Montevecchi, A. Scippa, and G. Campatelli, “Optimization of WAAM Deposition Patterns for T-crossing Features,” *Procedia CIRP*, vol. 55, pp. 95–100, 2016.

[71] M. C. Tsai, C. S. Chiou, J. S. Du, and J. R. Yang, “Phase transformation in AISI 410 stainless steel,” *Mater. Sci. Eng. A*, vol. 332, no. 1–2, pp. 1–10, 2002.

[72] E. J. Pavlina and C. J. Van Tyne, “Correlation of Yield strength and Tensile strength with hardness for steels,” *J. Mater. Eng. Perform.*, 2008.

[73] A.A.V.V., “Metallic materials — Tensile testing — Part 1: Method of test at room temperature,” 2016.

[74] A. Caballero, J. Ding, S. Ganguly, and S. Williams, “Wire + Arc Additive Manufacture of 17-4 PH stainless steel: Effect of different processing conditions on microstructure, hardness, and tensile strength,” *J. Mater. Process. Technol.*, vol. 268, no. April 2018, pp. 54–62, 2019.

[75] J. D. Verhoeven, “Steel Metallurgy for the Non-Metallurgist,” *ASM Int.*, no. January 2007, p. 203, 2007.

[76] M. Divya, C. R. Das, V. Ramasubbu, S. K. Albert, and A. K. Bhaduri, “Improving 410NiMo weld metal toughness by PWHT,” *J. Mater. Process. Technol.*, vol. 211, no. 12, pp. 2032–2038, 2011.

Appendix A

Technical Data Sheets

MIG/MAG WIRES (GMAW)
STAINLESS STEEL WIRES

OK Autrod 410NiMo

A continuous, solid welding wire of the 12% Cr, 4.5% Ni, 0.5% Mo type. OK Autrod 410NiMo is used for welding similar martentsitic and martensitic-ferritic steels in different applications, such as hydro turbines.

Classifications Wire Electrode:	EN ISO 14343-A:G 13 4

Typical Tensile Properties

Condition	Yield Strength	Tensile Strength	Elongation
As welded	860 MPa (125 ksi)	1050 MPa (152 ksi)	13 %
Stress relieved 2 hr 600 °C (1112 °F)	850 MPa (123 ksi)	900 MPa (130.5 ksi)	17 %
Stress relieved 8 hr 600 °C (1112 °F)	750 MPa (109 ksi)	850 MPa (123 ksi)	20 %

Typical Charpy V-Notch Properties

Condition	Testing Temperature	Impact Value
As welded	0 °C (32 °F)	35 J (26 ft-lb)
As welded	-20 °C (-4 °F)	30 J (22 ft-lb)
Stress relieved 2 hr 600 °C (1112 °F)	0 °C (32 °F)	70 J (52 ft-lb)
Stress relieved 8 hr 600 °C (1112 °F)	0 °C (32 °F)	75 J (55 ft-lb)
Stress relieved 2 hr 600 °C (1112 °F)	-20 °C (-4 °F)	55 J (40.5 ft-lb)
Stress relieved 8 hr 600 °C (1112 °F)	-20 °C (-4 °F)	75 J (55 ft-lb)

Typical Wire Composition %

C	Mn	Si	Ni	Cr	Mo	Cu
0.02	0.5	0.4	4.2	12.4	0.6	0.1

Deposition Data

Diameter	Current	Voltage	Wire Feed Speed	Deposition Rate
0.8 mm (.030 in.)	50-140 A	16-22 V	3.4-11 m/min (134-433 in./min)	0.8-2.7 kg/h (1.8-6.0 lb/h)
1.0 mm (.040 in.)	80-190 A	16-24 V	2.9-8.4 m/min (114-331 in./min)	1.1-3.1 kg/h (2.4-6.8 lb/h)
1.2 mm (3/64 in.)	180-280 A	20-28 V	4.9-8.5 m/min (193-335 in./min)	2.6-4.5 kg/h (5.7-9.9 lb/h)

Appendix B

WAAMPlanner Functions

- Slicer – divided in four functions, “Geo”, “Slice Point”, “Slice Plane” and “Layer Height”
    - Geo – used to select the CAD model which will be worked on;
    - Slice Plane – used to define the reference plane from where the slicing will be done, by picking three points. Can be viewed as the base of the deposited part or the top of the substrate;
    - Working Plane – used to select the position of the sliced layers in the Rhinoceros window by picking a point;
    - Layer Height – used to define the layer height. The user enters a numeric value, in mm, which will correspond to how much the torch will rise between layers.
- Sectioning – divided in five functions, “A”, “Dup”, “Meta”, DataFile” and “CustomZoneNumber”
    - A – simply used to connect the data from the Slice block to the Sectioning block;
    - Dup – short for Duplication, this is used by the software to determine how many layers will use the deposition parameters and shape currently selected;
    - Meta – used to select three basic deposition parameters. These parameters are, in order, the bead width of the oscillation path in mm, the wire feed speed in m/min and the diameter of the used wire in mm. The travel speed of the torch will be calculated based on these values;
    - DataFile – used to define a name for the file where the software will save the build data;
    - CustomZoneNumber – used to define how many custom zones will be used in Rhinoceros.
- PathMerger – divided in seven sections, although three share the same function. “A_Order”, “Reference Plane A”, “APP_A” share the same functions as “B_Order”, “Reference Plane B” and “APP_B”, with the latter being used when symmetrical building is carried out, which was not done at any point in this work, therefore they remain unused. “Do Merge” is the last function of this block
    - A_Order – used to define the order in which the previously created segments will be deposited;
    - Reference Plane A – has the same function as the Slice Plane present in the Slicer block;
    - APP_A – used to connect the data from the Sectioning block;
    - DoMerge – connected to a toggle button that instructs the program to continue to the next step when set to true.
- CPIGenerator – divided in five functions, “GrandPath”, “GenerateCPI”, “AMTech”, “AdjustFactor” and “ParametersSets”

- GrandPath – used to connect the data from the PathMerger block;
- GenerateCPI – has the same function as the DoMerge from the PathMerger block;
- AMTech – used to define the heat source of the welding process, with a value of “1” if a plasma source is used and “2” if CMT is employed;
- “AdjustFactor – used to define the ratio between the travel speed for the first layers and the travel speed used in the rest of the process. This is a technique used to compensate the cold temperature of the substrate in an initial stage of the deposition and provide more heat by slowing down the travel speed, ensuring an adequate deposition and bonding of the first layers with the substrate;
- ParameterSets – used to define the parameters for the custom zones created in Rhinoceros.

- KUKARC2CodeGenerator – divide in three functions, “GrandPath”, “GenerateKukaRC2Code” and “RobotSetup”. This block will generate a code which will be read by the robot.
  - GrandPath – used to connect the data from the CPIGenerator block;
  - GenerateKukaRC2Code – has the same function as the previously explained toggle functions;
  - RobotSetup – used to define the home position of the robot.